



# Enrichment of Circular RNA Expression Deregulation at the Transition to Recurrent Spontaneous Seizures in Experimental Temporal Lobe Epilepsy

Andreia Gomes-Duarte<sup>1</sup>, Sebastian Bauer<sup>2,3</sup>, Morten T. Venø<sup>4,5</sup>, Braxton A. Norwood<sup>6,7</sup>, David C. Henshall<sup>8,9</sup>, Jørgen Kjems<sup>4</sup>, Felix Rosenow<sup>2,3</sup>, Vamshidhar R. Vangoor<sup>1</sup> and R. Jeroen Pasterkamp<sup>1\*</sup>

<sup>1</sup> Affiliated Partner of the European Reference Network EpiCARE, Department of Translational Neuroscience, University Medical Center Utrecht Brain Center, University Medical Center Utrecht, Utrecht University, Utrecht, Netherlands, <sup>2</sup> Epilepsy Center Frankfurt Rhine-Main, Neurocenter, University Hospital Frankfurt and Center for Personalized Translational Epilepsy Research, Goethe-University Frankfurt, Frankfurt, Germany, <sup>3</sup> Epilepsy Center, Department of Neurology, Philipps University Marburg, Marburg, Germany, <sup>4</sup> Interdisciplinary Nanoscience Centre, Department of Molecular Biology and Genetics, Aarhus University, Aarhus, Denmark, <sup>5</sup> Omiics ApS, Aarhus, Denmark, <sup>6</sup> Department of Neuroscience, Expecor Inc., Kalispell, MT, United States, <sup>7</sup> Diagnostics Development, FYR Diagnostics, Missoula, MT, United States, <sup>8</sup> Department of Physiology and Medical Physics, Royal College of Surgeons in Ireland, Dublin, Ireland, <sup>9</sup> FutureNeuro, The Science Foundation Ireland Research Centre for Chronic and Rare Neurological Diseases, Royal College of Surgeons in Ireland, Dublin, Ireland

## OPEN ACCESS

### Edited by:

Amaresh Chandra Panda,  
Institute of Life Sciences (ILS), India

### Reviewed by:

Venkata Garikipati,  
The Ohio State University,  
United States  
Kotb Abdelmohsen,  
National Institute on Aging, National  
Institutes of Health (NIH),  
United States

### \*Correspondence:

R. Jeroen Pasterkamp  
r.j.pasterkamp@umcutrecht.nl

### Specialty section:

This article was submitted to  
RNA,  
a section of the journal  
Frontiers in Genetics

Received: 10 November 2020

Accepted: 06 January 2021

Published: 28 January 2021

### Citation:

Gomes-Duarte A, Bauer S, Venø MT, Norwood BA, Henshall DC, Kjems J, Rosenow F, Vangoor VR and Pasterkamp RJ (2021) Enrichment of Circular RNA Expression Deregulation at the Transition to Recurrent Spontaneous Seizures in Experimental Temporal Lobe Epilepsy. *Front. Genet.* 12:627907. doi: 10.3389/fgene.2021.627907

Mesial temporal lobe epilepsy (mTLE) is a common form of epilepsy and is characterized by recurrent spontaneous seizures originating from the temporal lobe. The majority of mTLE patients develop pharmacoresistance to available anti-epileptic drugs (AEDs) while exhibiting severe pathological changes that can include hippocampal atrophy, neuronal death, gliosis and chronic seizures. The molecular mechanisms leading to mTLE remain incompletely understood, but are known to include defects in post-transcriptional gene expression regulation, including in non-coding RNAs (ncRNAs). Circular RNAs (circRNAs) are a class of recently rediscovered ncRNAs with high levels of expression in the brain and proposed roles in diverse neuronal processes. To explore a potential role for circRNAs in epilepsy, RNA-sequencing (RNA-seq) was performed on hippocampal tissue from a rat perforant pathway stimulation (PPS) model of TLE at different post-stimulation time points. This analysis revealed 218 differentially expressed (DE) circRNAs. Remarkably, the majority of these circRNAs were changed at the time of the occurrence of the first spontaneous seizure (DOFS). The expression pattern of two circRNAs, circ\_Arhgap4 and circ\_Nav3, was further validated and linked to *miR-6328* and *miR-10b-3p* target regulation, respectively. This is the first study to examine the regulation of circRNAs during the development of epilepsy. It reveals an intriguing link between circRNA deregulation and the transition of brain networks into the state of spontaneous seizure activity. Together, our results provide a molecular framework for further understanding the role and mechanism-of-action of circRNAs in TLE.

**Keywords:** temporal lobe epilepsy, epileptogenesis, circular RNA, microRNA, network analysis, RNA-sequencing, early epilepsy

## INTRODUCTION

Epilepsy is considered the most common chronic brain disease and is estimated to affect more than 50 million people worldwide (Ngugi et al., 2010). Focal epilepsies account for 60% of all epilepsy forms (Devinsky et al., 2018). mTLE is a frequent form of focal epilepsy and is characterized by pathological manifestations that include hippocampal atrophy, neuronal death, gliosis and spontaneous seizures. Several factors have been identified as triggers that may lead to epilepsy, e.g., infectious agents, head trauma, brain tumors and genetic contributions (Duncan et al., 2006). While in the majority of patient symptoms can be controlled by AEDs, some patients do not become seizure-free and/or experience major adverse events in response to treatment (Wieser, 2004; Boon et al., 2009). In mTLE, the proportion of patients who do not become seizure free with AEDs is around 70–90% (Benbadis and Semah, 1999; Kurita et al., 2016). This condition, known as “refractory epilepsy,” highlights the need for the discovery of new molecular pathways that can be therapeutically targeted in TLE.

The molecular mechanisms underlying TLE remain incompletely understood (Dalby and Mody, 2001; Bender et al., 2004; Scimemi et al., 2006). Over the past years, a plethora of studies has shown that ncRNAs can influence various processes in the nervous system, including neuronal development, apoptosis, neurogenesis, oxidative stress, synaptic plasticity, and immune system activation, that are disturbed in the pathological process leading to mTLE (Henshall and Kobow, 2015; Henshall et al., 2016; Shao and Chen, 2017; Villa et al., 2019; Mills et al., 2020). In addition, experimental evidence highlights defects in post-transcriptional regulation in mTLE and the expression and function of different classes of ncRNAs is perturbed in experimental TLE and in TLE patients (Van Gassen et al., 2008; Jimenez-Mateos et al., 2012; Kan et al., 2012; Gong et al., 2018; Lee et al., 2018; Li J. et al., 2018; Guelfi et al., 2019; Fu et al., 2020; Gray et al., 2020; Venø et al., 2020). Together, these observations support the idea that ncRNAs may participate in the process of epileptogenesis. circRNAs are a class of ncRNA molecules that originate from back splicing events of a 5' splice

spite to an upstream 3' splice site leading to the formation of closed circular structures. The back splicing may occur directly in the primary transcript or in the event of ‘exon skipping,’ where back splicing occurs within the lariat product alongside mRNA production. Further, long introns and inverted repeats in flanking introns are known to potentiate circularization (Jeck and Sharpless, 2014). Due to their circular structure, which lacks a poly-A tail and 5'-cap structure, circRNAs are more resistant to degradation by most RNA decay mechanisms, leading to their accumulation over time (Cortés-López and Miura, 2016; Li X. et al., 2018). Although generally lowly expressed, studies have shown that circRNAs are highly enriched in the normal and diseased brain (Hansen et al., 2011; Rybak-Wolf et al., 2014; Hanan et al., 2017; Li X. et al., 2018). Further, even lowly abundant circRNAs can exert important physiological functions. For example, circ\_Spindr can promote axon regeneration upon peripheral nerve injury (Mao et al., 2019).

The mechanism-of-action of most circRNAs remains largely unexplored. Translation into polypeptides and selective interaction with miRNAs and RBPs are some of the currently reported functions of circRNAs (Li X. et al., 2018). Of these proposed functions, the ability of circRNAs to bind miRNAs via partial or full complementarity has been best-characterized. miRNAs can be involved in post-transcriptional regulation of multiple genes, generally by targeting their 3' UTRs. Ultimately, this interaction may lead to the activation of the RISC to promote directed miRNA target degradation (Bartel, 2009). Several studies propose a role for circRNAs in regulating miRNA-associated processes through sponging mechanisms, i.e., binding of miRNAs to circRNAs that will prevent these molecules from binding their messenger RNA targets (mRNA) (Hansen et al., 2013; Memczak et al., 2013; Thomas and Sætrom, 2014). It has therefore been proposed that circRNAs may control neuronal mechanisms by indirectly regulating, through miRNA sponging, the degradation or translation mRNA targets (Rong et al., 2017; Kristensen et al., 2019; Guria et al., 2020).

How circRNAs are regulated during the process of epileptogenesis remains unknown. To our knowledge, here we investigate for the first time how a specific circRNA/miRNA/mRNA network is deregulated at early stages of experimental epilepsy using a PPS rat model of TLE.

## MATERIALS AND METHODS

### Animal Experiments

All animal experiments were approved by local authorities in Marburg (Philips University Marburg, Germany: Regierungspraesidium Giessen, 73/2913) or in Utrecht (Animal Ethics Committee of Utrecht University) in compliance with Dutch laws (Wet op de Dierproeven, 1996; revised 2014). All procedures were performed in accordance with EU regulations (Guideline 86/609/EEC; Directive 2010/63/EU).

Male Sprague-Dawley rats (325–350 g; Charles River) were used in this study. Epilepsy was induced in rats using PPS, as previously described (Norwood et al., 2010; Costard et al., 2019).

**Abbreviations:** act-1, actin-1 precursor; AEDs, anti-epileptic drugs; BSJ, back-splice junction; CA1, *Cornu Ammonis* 1; CA3, *Cornu Ammonis* 3; *Cd200*, cluster of differentiation 200; cDNA, complementary DNA; ceRNAs, competitive endogenous RNAs; circRNA, circular RNA; Ct, cycle threshold; c.e., *C. elegans*; DE, differentially expressed; DG, dentate gyrus; dH<sub>2</sub>O, distilled water; DOFS, day of first spontaneous seizure; *Drd2*, dopamine receptor D2; FC, fold-change; FDR, false discovery rate; *Gapdh*, glyceraldehyde-3-phosphate dehydrogenase; GO, gene ontology; HS, hippocampal sclerosis; ILAE, International League Against Epilepsy; i.p., intraperitoneal; KEGG, Kyoto Encyclopedia of Genes and Genomes; log<sub>2</sub>FC, log<sub>2</sub>fold-change; miRNA, microRNA; MREs, microRNA response elements; mRNA, messenger RNA; mTLE, mesial temporal lobe epilepsy; ncRNAs, non-coding RNAs; NMD, nonsense mediated decay; padj, adjusted *p*-value; PCA, principal component analysis; PCR, polymerase chain reaction; PB, perforant pathway; PPS, perforant pathway stimulation; RBPs, RNA binding proteins; RISC, RNA-induced silencing complex; rn6, rat genome; RNA-seq, RNA-sequencing; Rnase R, ribonuclease R; rRNA, ribosomal RNA; RT-PCR, reverse transcriptase PCR; RT-qPCR, reverse transcriptase quantitative PCR; SD, standard deviation; SE, status epilepticus; SEM, standard error of the mean; TGF, transforming growth factor; TLE, temporal lobe epilepsy; *Tll1*, toll-like-1; UTRs, untranslated region;  $\beta$ -actin, beta-actin.

In short, an EEG transmitter (A3028R-FB, Open Source Instruments, Inc., Watertown, MA, United States) was implanted at the left abdominal site of the rat. Stimulation electrodes (diameter 0.125 mm, Plastics One, Roanoke, VA, United States) were implanted bilaterally into the angular bundle of PP, and recording electrodes (diameter 0.25 mm, Plastics One, Roanoke, VA, United States) were implanted bilaterally into the hilus of the DG. Electrode positions were verified by recording potentials evoked in the DG after PPS.

Starting immediately after surgery, video and EEG were recorded continuously (24/7) for up to 97 days. EEG recordings were performed using an Octal Data Receiver (A3027, Open Source Instruments, Inc., Watertown, MA, United States) with a sampling rate of 512/s. Data were recorded in NDF (Neuroscience Data Format) and converted to EDF (European Data Format) for analysis with EDFBrowser (version 1.57+). Video recording was performed with infrared cameras (IC-7110W, Edimax Technology, Willich, Germany) and sampled with SecuritySpy software (Ben Software Ltd., London, United Kingdom). The total EEG of all rats was screened visually for appearance of seizure patterns. Video was used to clarify appearance of artifacts (e.g., chewing, scratching).

After surgery, a 7-day recovery phase was allowed before bilateral PPS was applied on two consecutive days for 30 min and on the following day for 8 h. The 30 min stimulations on days 1 and 2 induce a state of epileptic tolerance which allows application of 8 h PPS on day 3 without causing self-sustaining status epilepticus or mortality. PPS was performed with a stimulus generator (Grass S88, Grass Telefactor/Grass Instruments, United States) and a stimulus isolator (Model SIU5, Grass Instruments, United States) using the following parameters: pulse duration 0.1 ms, frequency 2 Hz, voltage 20 V, twin pulses with interpulse interval of 40 ms, additional trains of 20 Hz single pulses at 20 V applied once per minute for 10 s. The animals develop mTLE with spontaneous seizure appearing after an average of  $19 \pm 11$  days (Costard et al., 2019). In addition, the animals develop HS ILAE type 1, which corresponds to the most frequently seen HS pattern in human mTLE (Norwood et al., 2010).

Rats were divided into six groups ( $n = 3$  rats per group) and were killed by transcardial perfusion with ice-cold PBS at different time points (days): 1 day, 3 days, and 10 days after epilepsy induction by PPS (epileptogenesis); on the day of the first spontaneous seizure (DOFS) (early epilepsy); 30 days after the first spontaneous seizure (chronic epilepsy); and 17 days after surgery (control group), as previously described (Venø et al., 2020). Hippocampi were stored at  $-80^{\circ}\text{C}$  until further use.

Wild-type Long Evans rats (7–10 g, Janvier Labs) were used to collect control material for RNase R experiments. Postnatal day 1 (P1) wild-type Long Evans rats were euthanized with Euthanimal 20% (50 mg/kg, i.p., Alfasan) and decapitated. Brains were quickly removed and hippocampi dissected and stored at  $-80^{\circ}\text{C}$ .

## Hippocampi RNA Extraction

Frozen hippocampal material was thawed on ice. RNA was obtained using Trizol purification as previously described (PPS

model rats) (Venø et al., 2020) or QIAzol lysis reagent with the miRNeasy Mini Kit (Qiagen) according to the manufacturer's instructions (wild-type Long Evans rats). Purified RNA was stored at  $-80^{\circ}\text{C}$  until library preparation (PPS model rats) or measured on Nanodrop (Thermo Fisher Scientific) and stored at  $-80^{\circ}\text{C}$  until RNase R experiments were performed (wild-type Long Evans rats).

## Library Preparation, RNA-Sequencing and circRNA Analysis

Purified RNA was rRNA depleted using the Ribo-Zero Magnetic Kit (human/mouse/rat; Illumina). Sequencing libraries were generated using the ScriptSeq v2 kit and sequenced as paired end 100 bp reads on an Illumina HiSeq 4000 sequencer and quality checked using 2100 Bioanalyzer analysis (Agilent). Sequencing data were preprocessed by removing adapter sequences and trimming away low quality bases (Phred score 20) with Trim Galore which uses the Cutadapt algorithm (Martin, 2011). CircRNA detection was performed by mapping filtered reads to the rat genome (rn6) with Bowtie (Langmead et al., 2009), using find\_circ (Memczak et al., 2013) to detect BSJ spanning reads from the reads that do not map linearly to the rat genome. Only circRNAs with two or more supporting BSJ reads within single samples were kept. A second circRNA detection algorithm, CIRCexplorer (Zhang et al., 2014), was used to verify the detected circRNAs. CIRCexplorer was guided by Ensembl Release 87 gene annotations on rat genome (rn6). Differential expression analysis was done using DESeq2 (Love et al., 2014) in R, limiting the analysis to the 1000 most highly expressed circRNAs, since these are the most likely to be biologically relevant. Raw counts of BSJ read numbers detected by find\_circ were used as input for DESeq2. Statistical metrics produced by DESeq2 including probability value ( $p$ -value,  $p$ ) and Benjamini–Hochberg adjusted  $p$ -values are reported with the normalized BSJ expression values generated by DESeq2. Detected circRNAs were checked for conservation in mouse and human by searching for expression of annotated mouse and human circRNAs with identical BSJ after conversion of mouse or human circRNA genomic regions (mm9 or hg19) from circBase<sup>1</sup> (Glažar et al., 2014) to rat genome (rn6) coordinates using the UCSC liftOver tool (Hinrichs et al., 2006). Homology% analysis was performed by considering the sequence of conserved human circRNAs (as defined by circBase) and using BLAT from UCSC genome browser to match human circRNA sequences to rat genome (Kent, 2002; Glažar et al., 2014). The homology is defined as [matching bp]/[total bp in circRNA]. The complete list of circRNAs detected after RNA-seq and DESeq2 analysis and their specifics can be found in **Supplementary Table 1**.

## RNase R Treatment, cDNA Synthesis, PCR and Real-Time PCR

Treatment with RNase R was performed for circRNA detection and validation of circularization. Briefly, 5  $\mu\text{g}$  of RNA derived from P1 rat hippocampus was diluted in 20  $\mu\text{l}$  of water

<sup>1</sup><http://circbase.org/>

containing 4 units/ $\mu\text{g}$  (U/ $\mu\text{g}$ ) of RNase R (Epicenter, Madison, WI, United States), 2  $\mu\text{l}$  of enzyme buffer (Epicenter) and 0,5  $\mu\text{l}$  of RiboLock RNase inhibitor (Thermo Fisher Scientific) followed by incubation for 20 min at 37°C. Retrotranscription of RNA material was performed with SuperScript IV First-strand Synthesis System (SSIV) (Thermo Fisher Scientific) as follows: 500 ng of RNase R treated or untreated RNA was retrotranscribed in a 20  $\mu\text{l}$  reaction mix according to the manufacturer's protocol and incubated for 10 min at 23°C, 10 min at 53°C and 10 min at 80°C. Semi-quantitative PCR for circularization confirmation following RNase R treatment was performed by amplifying 100 ng of cDNA with 0.3  $\mu\text{l}$  of TAQ<sup>TM</sup> DNA Polymerase (Qiagen), 2  $\mu\text{l}$  of 10x Reaction Buffer, 4  $\mu\text{l}$  of Buffer Q and 1.6  $\mu\text{l}$  of 10  $\mu\text{M}$  primers in a final 20  $\mu\text{L}$  reaction. Reactions were carried out according to the following program: 95°C for 2 min; 34 cycles at 95°C for 30 s, 60°C for 30 s, 72°C for 1 min and a final extension of 72°C for 10 min. 12  $\mu\text{l}$  of each PCR reaction were run on a 2% agarose gel (m/v) and analyzed using ImageJ software (Schneider et al., 2012). The intensity of each band was calculated as a numerical value meaning the brighter the band the higher the number. Resistance to RNase R treatment was calculated for each transcript as a ratio of the numerical values between the two groups (untreated and RNase R treated). Proof of circularity was defined for each circRNA if the fraction of the RNA expression recovered upon RNase R treatment was superior to the one recovered for the linear reference transcript, *beta-actin* ( *$\beta$ -actin*), with the same treatment.

cDNA used in quantitative real-time PCR (RT-qPCR) for intergroup quantification was processed with SSIV as mentioned above with an additional step. In this case, a spike-in RNA (an RNA transcript of known sequence derived from *Caenorhabditis elegans*) was added to each reverse transcriptase reaction for use in normalization. This allowed detection of possible cDNA synthesis artifacts which could interfere with fold-change (FC) calculations. 2 ng of each cDNA reaction were then used for amplification by RT-qPCR using FastStart Universal SYBR Green Master (Rox) (Sigma-Aldrich) in a QuantStudio<sup>(TM)</sup> 6 Flex System (Thermo Fisher Scientific). The RT-qPCR cycling conditions were as follows: 40 cycles of 95°C for 15 s, 60°C for 1 min and 95°C for 15 s followed by melting curve analysis. All cycle threshold (Ct) values  $\geq 35$  were considered background or amplification artifacts and discarded from further analysis. Relative expression levels of the analyzed genes were calculated using the  $2^{-\Delta\Delta\text{Ct}}$  method. For circRNA BSJ sequencing, RT-qPCR reactions were run in a 2% agarose gel (m/v), purified with PureLink<sup>TM</sup> Quick Gel Extraction Kit (Invitrogen) and further used for custom DNA sequencing (Standard-Seq) with circ\_Arhgap4 and circ\_Nav3 forward primers (F) (Macrogen).

We designed two different types of primer sets to be used in this study: convergent primers that bind linear mRNA transcripts and divergent primers, intended to bind circRNA molecules that are formed by 3'-5' back splicing events. All primers used in this study were designed either using the Primer-BLAST online tool<sup>2</sup> or selected from published literature (*Spidr*, *Cd200*) (Fonken et al., 2018; Mao et al., 2019) and

purchased from IDT-DNA (**Supplementary Table 2**). Two pairs of primers,  *$\beta$ -actin* and *Gapdh*, were used as housekeeping genes. NormFinder (\*.xla, MS Excel 2003 v0.953) was used to determine if a combination of housekeeping genes would be beneficial considering the experimental groups analyzed (Andersen et al., 2004) (**Supplementary Table 3**). Actin-1 precursor (act-1) primers were used for spike in detection.

## circRNA/miRNA/mRNA Network Construction

circRNA/miRNA/mRNA interaction networks were predicted and built according to a two-method sequential analysis. Initially, the freely accessible miRDB database (Chen and Wang, 2020) was used to predict both miRNA targeting sites in the circRNA sequences and subsequent mRNA targets of selected miRNAs. Targets retrieved from miRDB were predicted by a bioinformatics tool, miRTarget, that combines information from the analysis of multiple miRNA-target interactions from high-throughput sequencing experiments<sup>3</sup> (Liu and Wang, 2019). In our analysis, the custom prediction function of miRDB<sup>4</sup> (Chen and Wang, 2020) was used to predict annotated miRNAs with potential binding sites on circ\_Arhgap4 and circ\_Nav3 sequences in *Rattus norvegicus*. A target score of 60 was used as a threshold for the selection of the predicted miRNAs. Further, the previously selected miRNAs were used in the prediction of potential mRNA targets in *Rattus norvegicus*. Here, a target score of 80 was used as a threshold for target selection, as a prediction score greater than 80 is most likely to constitute a real interaction. The second step of the analysis included the construction of a network composed by the selected miRNA targets predicted during the first step of our pipeline. Cytoscape v\_3.7.2 was used to obtain a graphic representation of the circRNA/miRNA/mRNA molecular network (Shannon et al., 2003). All miRNAs (predicted target score > 60) were assigned as source nodes whereas all mRNAs (predicted target score  $\geq 80$ ) were assigned as target nodes during the network construction.

## Pathway Analysis of circRNA/miRNA/mRNA Genes

g:Profiler<sup>5</sup> (version e99\_eg46\_p14\_f929183) was used to perform functional profiling of the miRNA targets retrieved previously (Raudvere et al., 2019). g:Profiler output was then used for generating an Cytoscape EnrichmentMap representation of the main biological processes associated with the mRNA network, according to a published pipeline (Reimand et al., 2019).

The enrichment analysis of target genes in biologically relevant pathways was performed with Cytoscape StringApp (Shannon et al., 2003; Doncheva et al., 2019). StringApp uses information from open-source databases to retrieve networks and functional enrichment analysis by combining several selective categories (GO, InterPro Domains, KEGG Pathways, Reactome Pathways, PFAM Domains, etc.). In this study, the

<sup>3</sup><http://www.mirdb.org>

<sup>4</sup><http://www.mirdb.org/custom.html>

<sup>5</sup><https://biit.cs.ut.ee/gprofiler/gost>

<sup>2</sup><https://www.ncbi.nlm.nih.gov/tools/primer-blast/>

STRING: protein query public database was used as data source (Doncheva et al., 2019). The enrichment score associated with each category was calculated as the negative logarithm of the FDR value. The most significant sorted FDR values were used as criteria for the statistical significance of the enrichment found. Relevant genes of interest and corresponding most significant enrichment processes were used for the visual representation of the pathway analysis using Cytoscape StringApp, as described previously.

## Statistical Analysis

GraphPad Prism 8 was used to assess statistical significance for RT-qPCR analysis, which was performed using an unpaired two-tailed Student's *t*-test;  $n = 3$  animals per group. Statistical significance was considered for  $p < 0.05$  (\*\*\*\* $p < 0.0001$ ; \*\*\* $p < 0.001$ ; \*\* $p < 0.01$ ; \* $p < 0.05$ ; not significant, ns:  $p \geq 0.05$ ). All values were expressed as mean  $\pm$  standard error of the mean (SEM) with the exception of RNase R experiments, in which standard deviation (SD) was used to better represent the variation between independent experiments.

Cytoscape StringApp was used to perform and graphically represent GO analysis results. The FDR method was used in all analyses as a correction for multiple testing according to the Benjamini-Hochberg procedure. Statistical significance was considered for  $FDR < 0.05$ .

## RESULTS

### Spatiotemporal circRNA Expression in a Rat PPS Model of mTLE

The rat PPS model was used to profile circRNA expression at different stages during the process of epileptogenesis leading to spontaneous seizures and epilepsy (Figure 1A). In this model, seizure activity is provoked and maintained throughout the stimulation process without promoting convulsive SE (Norwood et al., 2011). *In vivo* PPS is characterized by high survival rates and low variability of hippocampal injury while displaying major pathophysiological hallmarks of mTLE, such as hippocampal atrophy, gliosis, hippocampal region-specific neuronal death resembling ILAE type 1, and recurrent spontaneous seizures (Norwood et al., 2010).

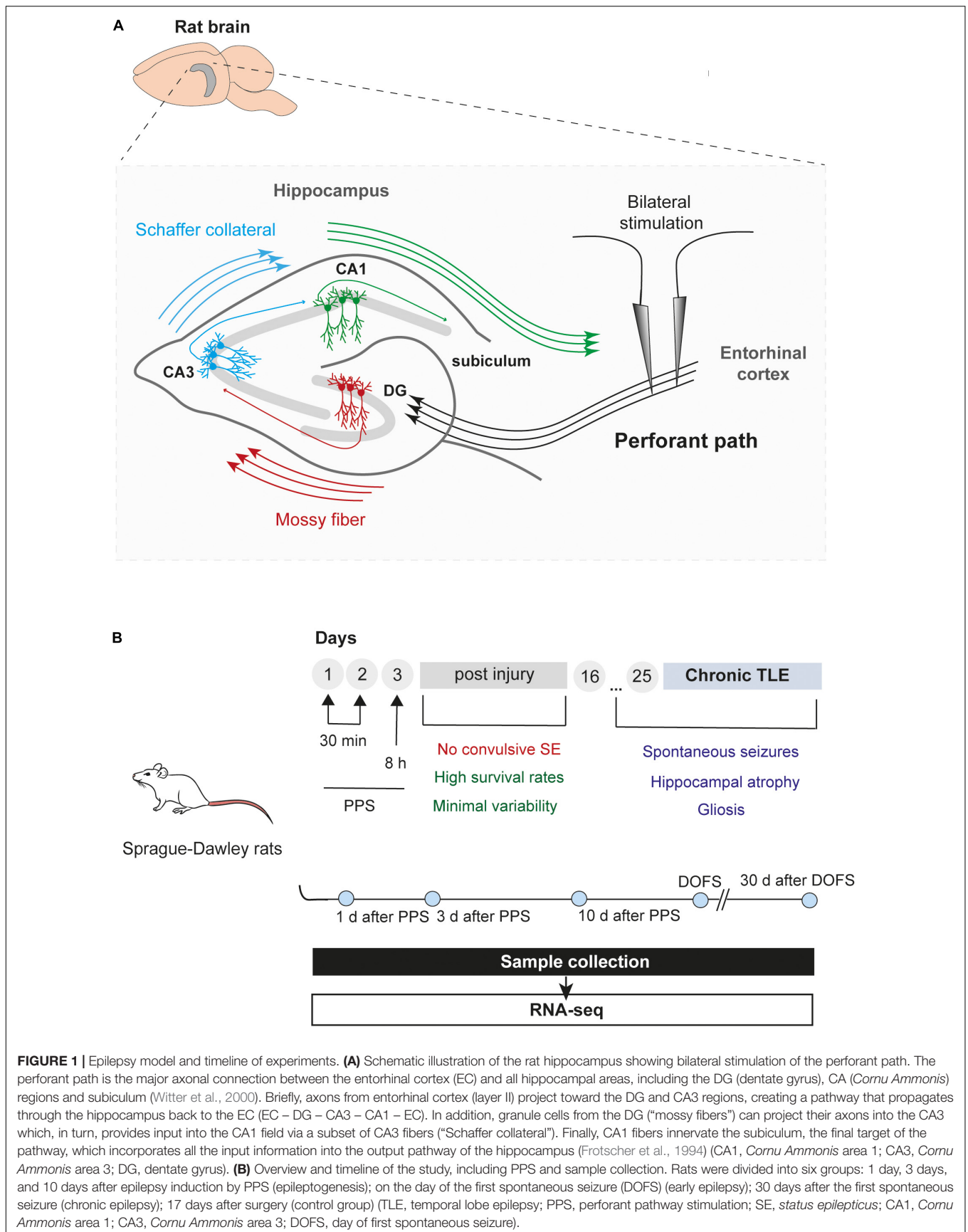
High-throughput sequencing of rat hippocampi was performed at the following time points: 1 day, 3 days, and 10 days after PPS (epileptogenesis), at the day of the first spontaneous seizure (DOFS) after PPS (early epilepsy), and 30 days after DOFS (chronic epilepsy); 17 days after surgery (control group) (Figure 1B). In total, 22811 circRNAs were identified in both the control and PPS groups. Considering the very low level of expression of several detected circRNAs only the 1000 most highly expressed circRNAs were used in further analyses. Of these, 771 were classified as exonic and 229 classified as intergenic (Figure 2A). Among the exonic circRNAs, the majority was composed of more than one exon (88%), while only 90 (12%) were single exon circRNAs (Figure 2A). Considering the length of exonic circRNAs, a large number of circRNAs (62.6%) had a size smaller than 500 bp, while a small

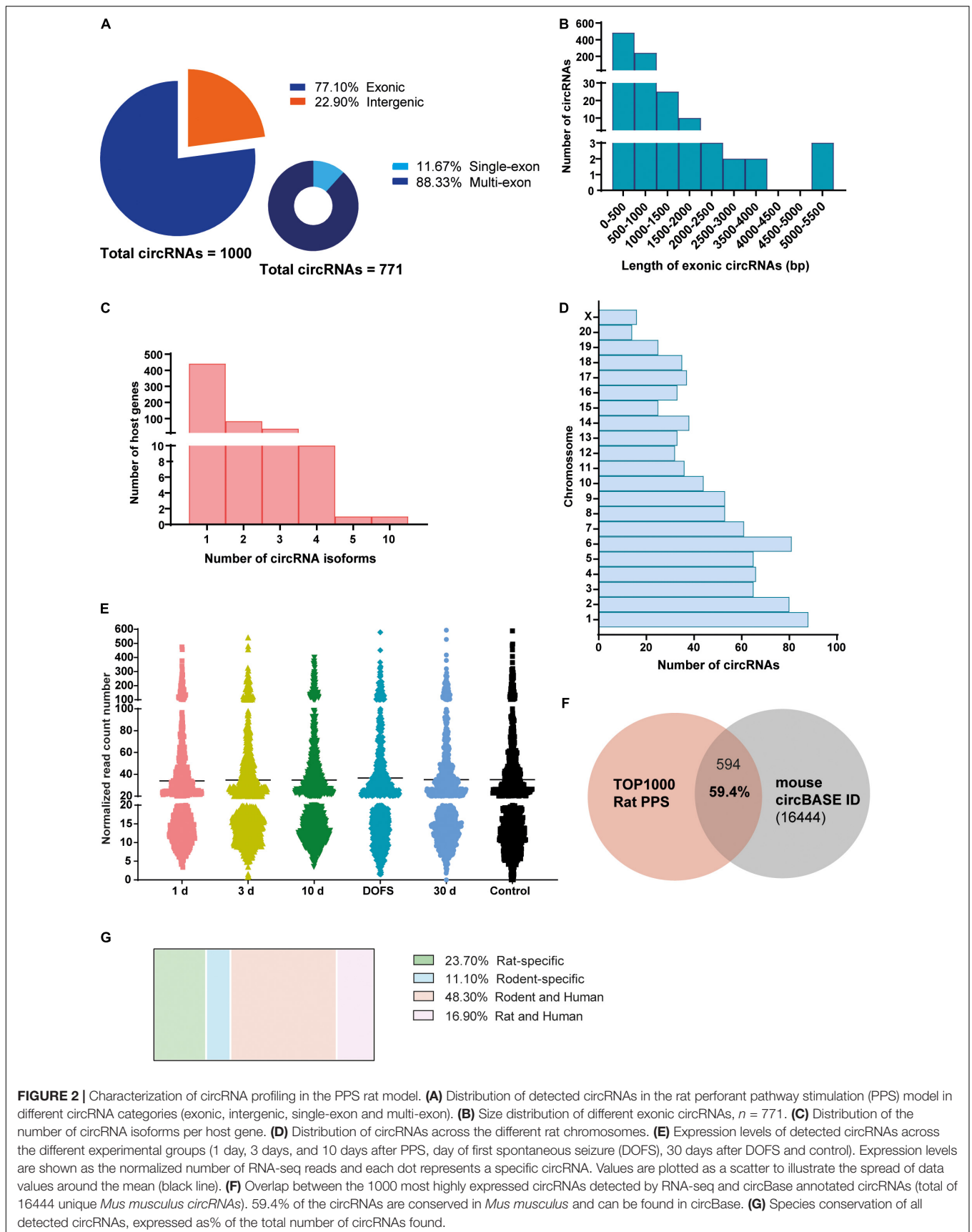
fraction of circRNAs (1.4%) was over 2000 bp (Figure 2B). These numbers are within the size range previously described for exonic circRNAs (>100 nt to <4 kb) (Lasda and Parker, 2014). In addition, most circRNAs derived from genes that give rise to a single circRNA isoform (77%), as opposed to multiple different isoforms (Figure 2C). The detected circRNAs were present and widely distributed across all rat chromosomes, with exception of the Y chromosome (Figure 2D). This phenomenon has been described by others (Li J. et al., 2018) and might be explained by the low gene density of the Y chromosome across organisms, with the majority of its sequence being composed of non-coding repetitive genome regions that do not produce exonic transcripts (Lluís and Fellous, 2001; Ovcharenko et al., 2005). The majority of detected circRNAs were expressed at low levels at all experimental time points ( $\leq 100$  normalized read counts) (Figure 2E). Of all circRNAs, 59.4% of the circRNAs were conserved in mouse and had their circRNA ID annotated in the circBase database (Figure 2F). In contrast to previous observations (Rybak-Wolf et al., 2014), only a small portion of the rat circRNAs detected here had a conserved human isoform (16.9%) and a considerable fraction of circRNAs (23.7%) were rat-specific (Figure 2G).

Out of the 1000 most highly expressed circRNAs, 218 were found to be significantly differentially expressed (DE) across time points ( $p < 0.05$ ) (Figure 3). Most of these 218 circRNAs were also detected by CIRCexplorer, in addition to find\_circ (Figure 3). This validation by a second circRNA detection algorithm is important, as annotations for rat genes are currently less well developed as compared to those of for example mouse or human. Only circRNAs detected by both CIRCexplorer and find\_circ algorithms were taken into consideration for further experimental analysis.

### Analysis of Differentially Expressed circRNAs at the Day of First Spontaneous Seizure (DOFS)

The circRNA transcriptomes of the six experimental groups were compared using PCA. This showed that although there is overlap between several groups, a clear separation could be observed between the control and DOFS groups (Figure 4A). This observation is supported by the number of DE circRNAs at the different time points. The largest number of DE circRNAs was found at the DOFS, followed by 3 days and 10 days after PPS groups. A similar distribution of DE RNAs was found when analyzing the mRNA transcriptome, which showed the highest number of DE genes at early stages (DOFS and 1 day after PPS) of experimental epilepsy (Figure 4B). Furthermore, our analysis revealed a trend for an overall lower circular-to-linear ratio, i.e., the presence of more mRNA molecules as compared to circRNA molecules per gene (Figure 4C). Considering the observation that major changes in the (non-)coding transcriptome occur at the DOFS, we performed further analyses at this time point. Interestingly, at the DOFS, expression of most circRNAs was linked to host mRNA expression. Nevertheless, a few circRNA changes appeared to be independent of their linear counterparts suggesting that circRNA deregulation is in part uncoupled





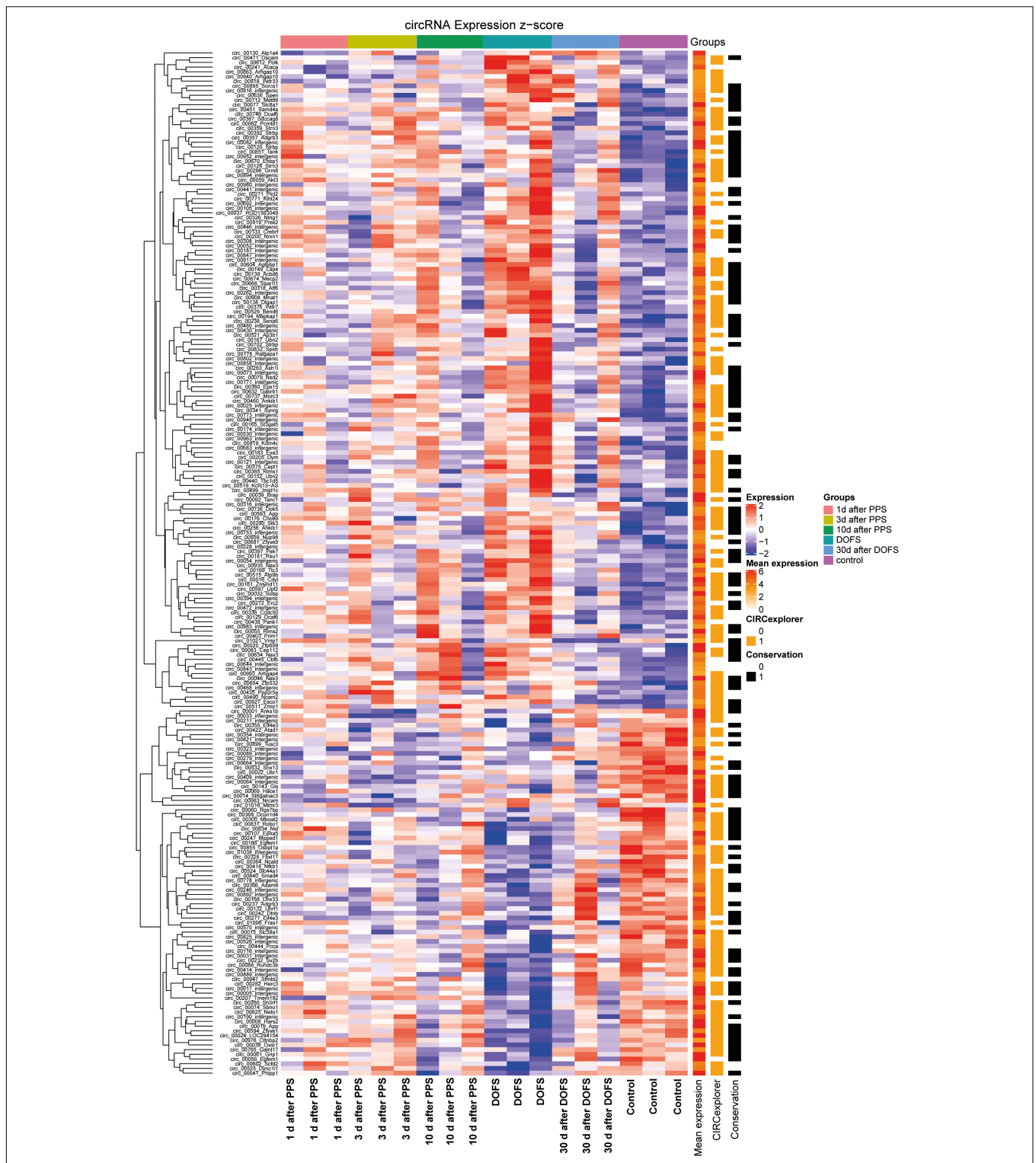


**FIGURE 3 |** Differentially expressed circRNAs. Heatmap representation of circRNA detection, conservation and expression in the different experimental groups [1 day, 3 days, and 10 days after performant pathway stimulation (PPS); day of first spontaneous seizure (DOFS) and 30 days after DOFS; control]. All circRNAs with FDR < 0.05 for any time point relative to control group are shown. Expression (z-score) of each circRNA is represented in each cell, where z-score represents the number of standard deviations away from the mean [from -2 (blue) to 2 (red)]. Mean expression shows expression of each individual circRNA across all samples in log scale [low expression (white), medium expression (orange) or high expression (red)]. CIRCexplorer indicates if a specific circRNA is also found by the CIRCexplorer algorithm [found by CIRCexplorer (orange) or not (uncolored)]. Conservation specifies if a circRNA is conserved to mouse, according to circBase [conserved (black) or not conserved (uncolored)].

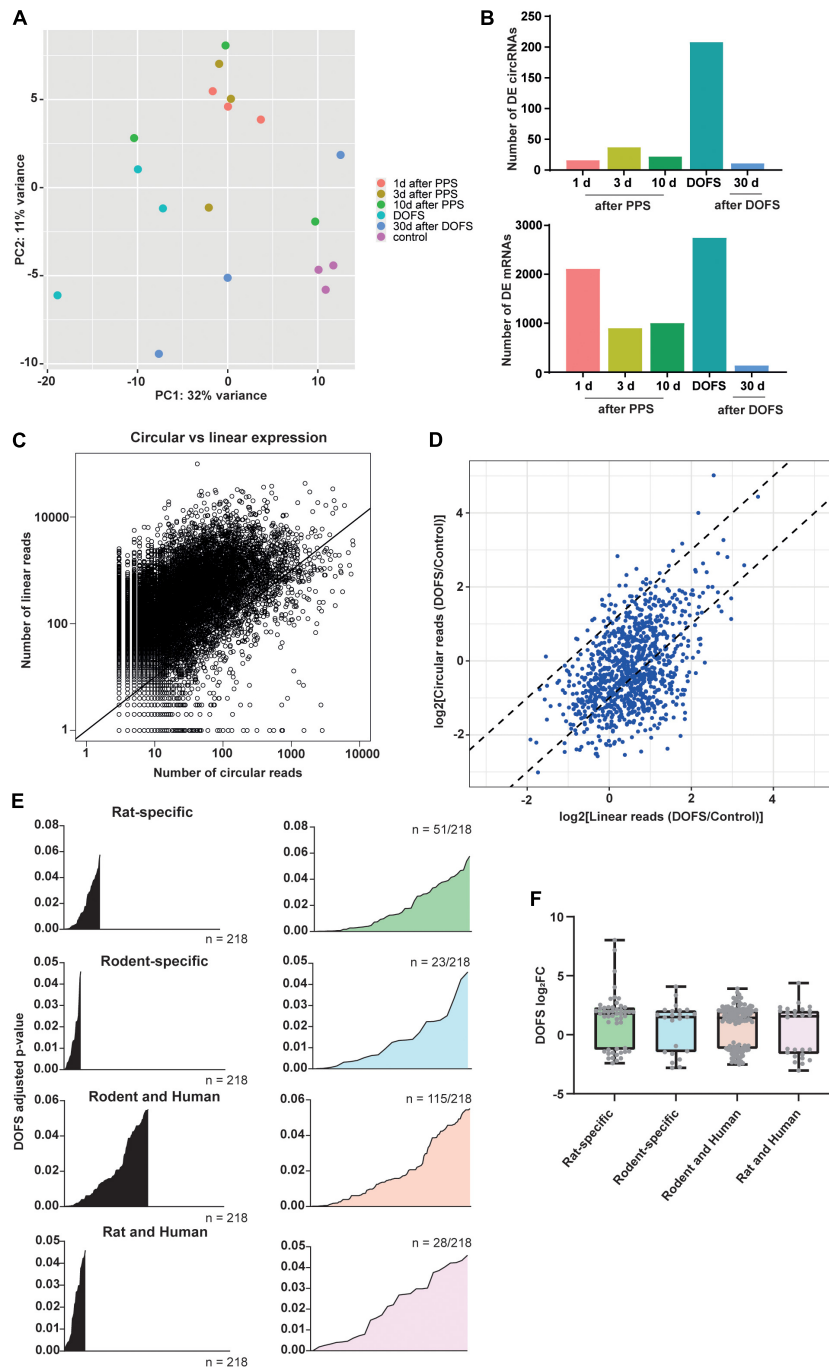


**FIGURE 4 |** Transcriptome characterization at DOFS. **(A)** Principal component analysis (PCA) of the different experimental groups based on the transcriptome changes of the 1000 most highly expressed circRNAs. **(B)** Number of differentially expressed circRNAs (upper panel) and mRNAs (lower panel) at the six experimental time points ( $p < 0.05$ ) (DE, differentially expressed). **(C)** Scatter plot showing the comparison of circRNA and mRNA expression. The x-axis shows the number of reads mapped across the back-splice junction (BSJ) for each detected circRNAs; the y-axis shows the number of linearly spliced reads from the corresponding splice acceptor and splice donor sites. Each dot represents one host gene and corresponding circRNA expression. The diagonal black line separates circRNAs that are expressed lower than linear host gene transcripts (above the line) from circRNAs that are expressed higher than linear host gene transcripts (below the line). **(D)** Circular and linear transcript regulation at the DOFS. Axis represent the DOFS/Control ratio for linear (x-axis) and circular (y-axis) reads. Each dot depicts one circRNA. Dotted lines indicate twofold changes ( $-2$  to  $2$ ) and show if differences between control and DOFS impact linear and circular expression equally (in between the two dotted lines) or independently (outside the two dotted lines). **(E)** Statistical significance distribution of the 218 significantly deregulated circRNAs within the three conservation classes (rat-specific =  $51/218$ , rodent-specific =  $23/218$ , rodent and human =  $115/218$ , rat and human =  $28/218$ ). **(F)** Distribution of the  $\log_2\text{FC}$  values of the 218 significantly deregulated circRNAs within the three conservation classes (rat-specific, rodent-specific, rodent and human, rat and human). Each dot depicts one circRNA ( $\log_2\text{FC}$ ,  $\log_2$ fold-change).

from host gene expression at the DOFS (Figure 4D). The statistical values of the DE circRNAs at the DOFS were found to be homogeneously distributed over the different categories of species-specific circRNAs (rat-specific, rodent-specific, rodent and human, rat and human) (Figure 4E).

## Differentially Expressed circRNA Selection and Validation

The most prominent deregulation of circRNA expression in the PPS model was observed for rat-specific circRNAs at early stages of epilepsy (DOFS) (Figure 4F). A  $\log_2$  fold-change ( $\log_2FC$ ) parameter was used as a filtering criterion to select potential circRNA candidates ( $\log_2FC \geq 2$  or  $\leq -2$ ). This yielded a total of 20 circRNAs (Table 1) which show a similar pattern of deregulation at the different time points and a marked expression change at the DOFS (Figure 5A). Four candidates (three upregulated and one downregulated) were selected for further validation based on the differential expression between the DOFS and control groups. All of the four selected circRNAs fall into the most common length categories of overall RNA-seq transcripts, with an exonic size below 550 bp. For the selected circRNAs, exon number appeared to be related to the size of the circRNA, with larger circRNAs containing more exons (Figure 5B). Next, we used two circRNA detection bioinformatics tools (“find\_circ” and “CIRCexplorer”) to predict the BSJ and further allow circRNA detection (Figure 5C). First, circularity of the four selected circRNAs was assessed by PCR across the BSJ and by RNase R treatment of P1 rat hippocampus RNA. The selected circRNAs were resistant to digestion by RNase R in contrast to a linear reference transcript,  $\beta$ -actin, supporting the circular structure of these transcripts (Figure 5D).

Next, the relative expression levels of the four selected circRNAs were validated in control and DOFS rat samples using qRT-PCR and divergent primer sets. This qRT-PCR analysis was generally in line with the RNA-seq data. Specifically, circ\_Arhgap4 and circ\_Nav3 were found to be significantly upregulated in the DOFS group (circ\_Arhgap4,  $***p = 0.0005$ ; circ\_Nav3,  $**p = 0.0038$ ) as compared to control (Figure 5E). Although circ\_Spidr and circ\_Neto1 also appeared to be deregulated, these changes were not statistically significant (Figure 5E). The linear host transcripts for circ\_Arhgap4, circ\_Nav3 and circ\_Neto1 were significantly increased (Arhgap4,  $*p = 0.0354$ ; Nav3,  $****p < 0.0001$ , Neto1,  $*p = 0.0124$ ) at DOFS (Figure 5F).

## circRNA/miRNA/mRNA Networks

As upregulation of circ\_Arhgap4 and circ\_Nav3 at the DOFS was confirmed by qRT-PCR we further focused on these circRNAs. We performed custom DNA sequencing of circ\_Arhgap4 and circ\_Nav3 BSJs as an extra validation of their sequences, which confirmed the RNA-seq annotations (Supplementary Figures 1A,B). Next, we examined possible downstream effects of circ\_Arhgap4 and circ\_Nav3 upregulation at the DOFS. Accumulating evidence reports a role for circRNAs in regulating gene expression via specific circRNA/miRNA/mRNA-associated networks (Rong et al., 2017; Kristensen et al., 2019; Guria et al., 2020). This results from the ability of circRNAs to compete with mRNAs for miRNA binding via miRNA response elements (MREs) (Hansen et al., 2013; Memczak et al., 2013; Thomas and Sætrum, 2014). Therefore, miRDB was used to predict miRNA binding sites in the selected circRNAs. Given the circular nature of circRNA transcripts and their rat-specificity, the custom prediction tool from miRDB was used to obtain the

**TABLE 1** | List of most differentially expressed circRNAs between control and DOFS groups.

| circRNA             | DOFS $\log_2FC$ | P-value | Genomic region            | Host gene description                                                    |
|---------------------|-----------------|---------|---------------------------|--------------------------------------------------------------------------|
| circ_00993_Arhgap4  | 7.17            | 0.0032  | chrX:156882943–156884142  | Rho GTPase activating protein 4                                          |
| circ_00935_Nav3     | 4.38            | 0.0002  | chr7:52223221–52248773    | Neuron navigator 3                                                       |
| circ_00832_Spidr    | 3.18            | 0.0034  | chr11:89175424–89180448   | Scaffold protein involved in DNA repair                                  |
| circ_00612_Polk     | 2.71            | 0.0004  | chr2:27326040–27333634    | DNA polymerase Kappa                                                     |
| circ_00746_Dcaf6    | 2.70            | 0.0026  | chr13:83601156–83607039   | DDB1 and CUL4 Associated Factor 6                                        |
| circ_00199_Ttc3     | 2.45            | 0.0007  | chr11:34611538–34614139   | Tetratricopeptide repeat domain 3                                        |
| circ_00167_Ubn2     | 2.37            | 0.0040  | chr4:66172554–66232564    | Ubiquitin 2                                                              |
| circ_00918_Wdr33    | 2.33            | 0.0158  | chr18:24611732–24614740   | WD repeat domain 33                                                      |
| circ_00597_Upf2     | 2.33            | 0.0046  | chr17:76245626–76265943   | Regulator of nonsense transcripts 2                                      |
| circ_00863_Arhgap10 | 2.32            | 0.0125  | chr19:34249086–34272145   | Rho GTPase activating protein 10                                         |
| circ_00959_Nup98    | 2.19            | 0.0268  | chr1:167260357–167269761  | Nucleoporin 98 and 96 precursor                                          |
| circ_00529_Bend6    | 2.15            | 0.0042  | chr9:38321691–38326937    | BEN domain containing 6                                                  |
| circ_00163_Eya3     | 2.14            | 0.0005  | chr5:150850431–150865550  | Eyes absent homolog 3                                                    |
| circ_00919_Prex2    | 2.08            | 0.0390  | chr5:7703775–7780390      | Phosphatidylinositol-3,4,5-trisphosphate dependent Rac exchange factor 2 |
| circ_00403_Prim1    | 2.03            | 0.0422  | chr7:2440627–2448053      | DNA primase subunit 1                                                    |
| circ_00440_Tbc1d5   | 2.01            | 0.0402  | chr9:1442053–1485363      | TBC1 domain family member 5                                              |
| circ_00444_Pcca     | –2.46           | 0.0018  | chr15:109127706–109141568 | Propionyl-CoA carboxylase subunit alpha                                  |
| circ_00625_Neto1    | –2.41           | 0.0072  | chr18:83542805–83556790   | Neuropilin and tolloid like 1                                            |
| circ_00947_Sfmbt2   | –2.21           | 0.0377  | chr17:71875847–71886141   | Scm like with four Mbt domains 2                                         |
| circ_00602_Scfd2    | –2.15           | 0.0147  | chr14:36341463–36341713   | Sec1 family domain containing 2                                          |

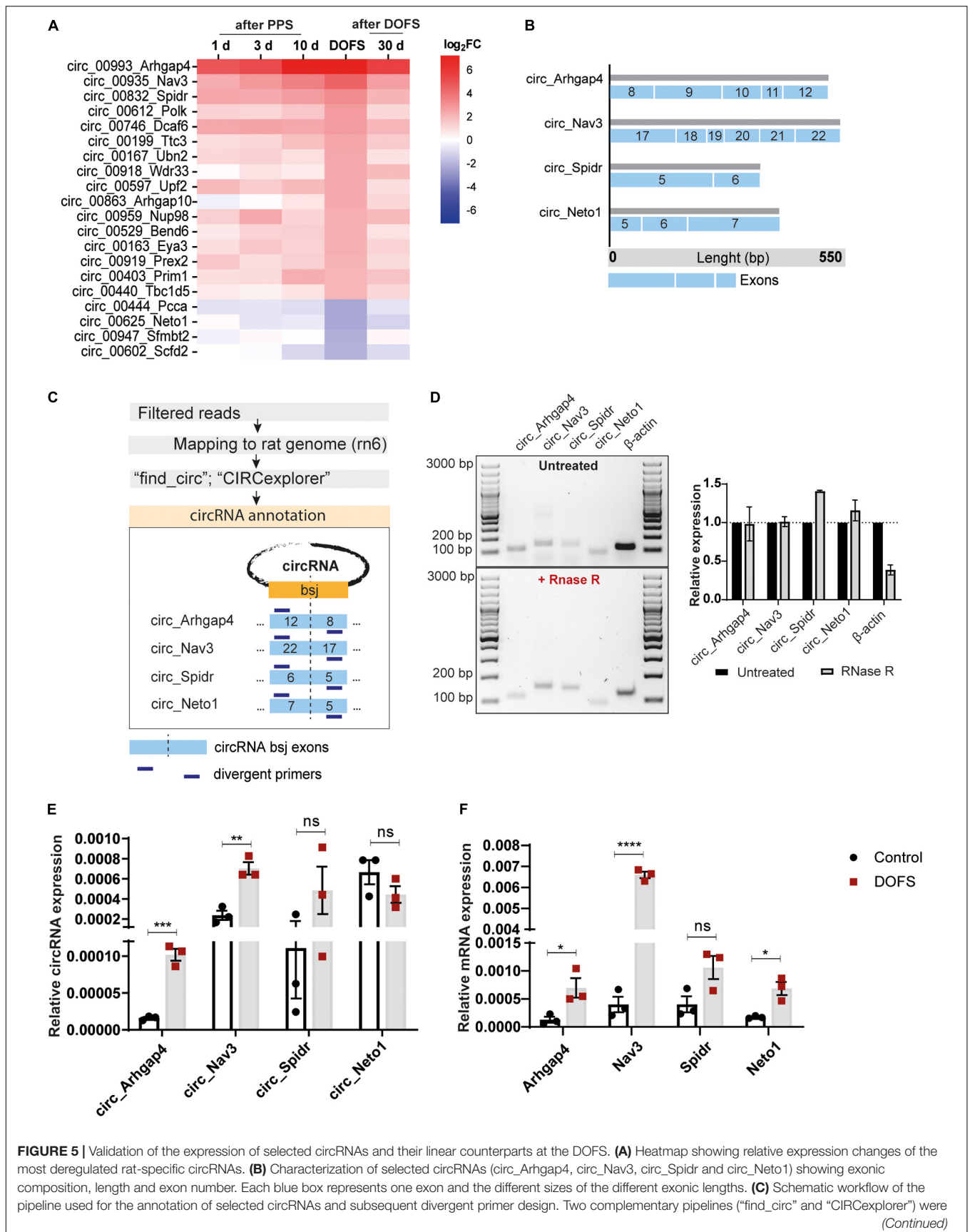


**FIGURE 5 |** Validation of the expression of selected circRNAs and their linear counterparts at the DOFS. **(A)** Heatmap showing relative expression changes of the most deregulated rat-specific circRNAs. **(B)** Characterization of selected circRNAs (circ\_Arhgap4, circ\_Nav3, circ\_Spidr and circ\_Neto1) showing exonic composition, length and exon number. Each blue box represents one exon and the different sizes of the different exonic lengths. **(C)** Schematic workflow of the pipeline used for the annotation of selected circRNAs and subsequent divergent primer design. Two complementary pipelines (“find\_circ” and “CIRCexplorer”) were (Continued)

**FIGURE 5 |** Continued

used for the annotation of circRNA sequences. The BSJ of each circRNA was defined as a 100 bp junction between the last and first circRNA exon (blue box). Divergent primers were designed against this region for each circRNA (bsj, back-splice junction). **(D)** Agarose gel electrophoresis of the PCR products from circRNA back-splice junction amplification with (upper panel) and without (lower panel) RNase R treatment. Original images were color inverted for improved visualization. Quantification of RNA expression is shown in the right panel. Values are expressed as the mean  $\pm$  SD. RNase R-treated expression is normalized to the untreated condition ( $n = 2$  independent experiments) (bp, base pairs). **(E)** RT-qPCR analysis of the expression pattern of circRNAs at DOFS (circ\_Arhgap4, \*\*\* $p = 0.0005$ ; circ\_Nav3, \*\* $p = 0.0038$ ; circ\_Spidr, ns; circ\_Neto1, ns). The bar plots represent circRNA expression relative to  $\beta$ -actin and Gapdh. Values are expressed as the mean  $\pm$  SEM,  $p < 0.001$ : \*\*\*,  $p < 0.01$ : \*\*,  $p \geq 0.05$ : ns (unpaired two-tailed Student's  $t$ -test,  $n = 3$  animals per group). **(F)** RT-qPCR analysis of the expression pattern of circRNAs' linear counterparts at DOFS (Arhgap4, \* $p = 0.0354$ ; Nav3, \*\*\*\* $p < 0.0001$ ; Spidr, ns; Neto1, \* $p = 0.0124$ ). The bar plots represent mRNA expression relative to  $\beta$ -actin and Gapdh. Values are expressed as the mean  $\pm$  SEM,  $p < 0.0001$ : \*\*\*\*,  $p < 0.05$ : \*,  $p \geq 0.05$ : ns (unpaired two-tailed Student's  $t$ -test,  $n = 3$  animals per group).

predicted sequences of miRNA interactions with the circRNA spliced sequence, including the back-splice region. Circ\_Arhgap4 and circ\_Nav3 harbored five or one, respectively, predicted miRNA sites and one to three binding sites for each miRNA (**Supplementary Table 4**). A miRDB prediction score  $> 60$  was considered as an inclusion criterion and following application of this cutoff one and two miRNAs were selected for circ\_Arhgap4 (*rno-miR-6328* and *rno-miR-1306b-5p*) and circ\_Nav3 (*rno-miR-10b-3p*) (**Figure 6A**). We further performed target prediction analysis to identify potential targets of the selected miRNAs. After applying a prediction score threshold  $\geq 80$ , an average of 25 mRNA targets were found for each miRNA (**Figure 6B**) (listed in **Supplementary Table 4**). One mRNA target, *tolloid-like-1* (*Tll1*) was shared between the potential miRNA binding partners of circ\_Nav3 and circ\_Arhgap4. Next, we probed the involvement of predicted circRNA/miRNA targets in key biological processes. g:Profiler was used to perform functional enrichment of the mRNA targets. Retrieved GO categories were grouped based on a higher level of clustering and graphically represented using EnrichmentMap Cytoscape App (**Figure 6C**). Full annotations and subsequent clustering are listed in detail in **Supplementary Table 5**. Signaling, response to stimulus and regulation of biological processes, development and morphogenesis, neurogenesis, nervous system development and synapse regulation were found to be among the most significant pathways associated with the circRNA/miRNA targets (**Figure 6C**).

circRNA/miRNA interactions have been proposed to control miRNA availability and therefore indirectly control the expression of downstream miRNA targets (Panda, 2018). Enhanced expression of a circRNA may therefore result in decreased availability of miRNAs and thereby increased expression of mRNAs targeted by these miRNAs. To test this hypothesis for the circRNAs studied here, the expression of three miRNA targets was assessed by qRT-PCR in control and DOFS samples. *Tll1*, *dopamine receptor D2* (*Drd2*) and *cluster of differentiation 200* (*Cd200*) were selected because of their reported link to epilepsy, shared interactions and molecular functions (**Table 2**). Consistent with the proposed model, expression of the three mRNA targets was increased at the DOFS, although this effect was only statistically significant for *Drd2* as compared to control (**Figure 7A**). *Drd2* is one of the top circ\_Arhgap4:miR-6328 target genes (target score = 83). Further, it was found to be enriched in all of the 24 GO terms retrieved for the miRNA target gene set (**Supplementary Table 5**). StringApp

was used to functionally characterize and visually represent *Drd2* in three categories: GO Molecular Function, Reactome and KEGG Pathways. This approach allowed an integrative perspective of *Drd2* functions while considering *Drd2* protein interactions with the remaining miRNA targets in the network (pp). All results from the *Drd2* network analysis are listed in **Supplementary Table 6**. The most representative categories linked to *Drd2* included protein binding, binding to glutamate receptor, ion binding, GPCR downstream signaling, G alpha (i) signaling events, neuroactive ligand-receptor interaction, and dopaminergic synapse (**Figure 7B**). Moreover, *Drd2* can act as an effector with additional functions in different pathways (G-protein alpha-subunit binding, Ras activation upon  $Ca^{2+}$  influx through NMDA receptor, downstream signaling events of B Cell receptor and neurotrophin signaling pathway) via pp interactions with other network targets (**Figure 7B**). Overall, the functional characteristics of the *Drd2* network are mainly associated with the intracellular transduction of extracellular signals (ion binding, GPCR activation or neurotrophin signaling), key players in processes like memory, learning and synaptic plasticity (Reichardt, 2006; Voglis and Tavernarakis, 2006; Calebiro et al., 2010). A closer inspection of the retrieved GO categories revealed both glutamate and dopamine signaling. Glutamate receptors are the main excitatory mediators in the brain and their overactivation has been associated with epileptogenesis (Barker-Haliski and Steve White, 2015). Additionally, dopaminergic receptors are known to play a role in the modulation of seizures that originate in the limbic system (Bozzi and Borrelli, 2013). The above described bioinformatics results suggest an important role for *Drd2* in initiating a physiological response in the brain and, particularly, during epileptogenesis.

## DISCUSSION

The search for novel and effective therapeutic targets for the treatment of epilepsy is a priority in the field. In the past years, increasing experimental evidence has identified ncRNAs as potential therapeutic targets in epilepsy (Henshall and Kobow, 2015; Shao and Chen, 2017; Mills et al., 2020). Different types of ncRNAs exist and here we focused on circRNAs, a recently rediscovered class of ncRNAs, with enriched expression in the brain and the ability to regulate gene expression via different mechanisms. Thus far, studies on the role of circRNAs in epilepsy have focused on chronic stages of TLE, both in patient samples

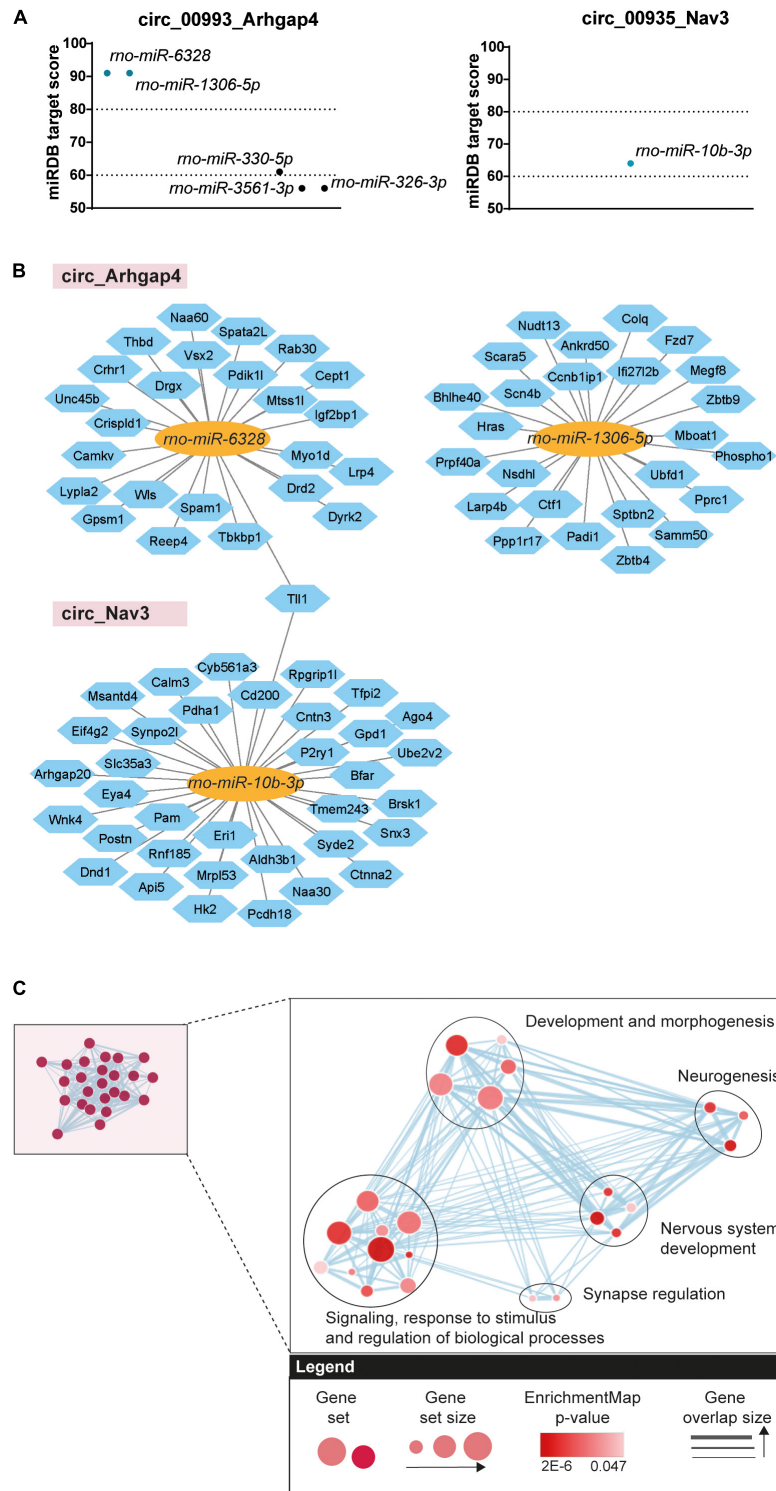


**FIGURE 6 |** Bioinformatics analysis of circRNA/miRNA networks. **(A)** Predicted miRNA targets of circ\_Arhgap4 and circ\_Nav3 (miRDB predicted score > 60). Dotted lines represent high confidence (miRDB predicted score = 80) and minimum confidence (miRDB predicted score = 60) thresholds used in further selection. **(B)** Diagram showing predicted mRNA targets derived from the circRNA/miRNA (miRDB analysis, predicted score > 80). circRNAs are represented by the pink rectangles; predicted bound miRNAs by the yellow ovals and miRNA targets by the blue hexagons. **(C)** Cluster representation of GO biological processes associated with the selected circRNA/miRNA interactions. Different GO categories were assigned into clusters according to their biological function. Each black circle represents a cluster; the colored circles represent groups of genes enriched in a certain GO category; the size of the circle denotes the number of genes composing that GO category; the color gradient shows significance and the gray arrows represent gene overlap between categories (FDR < 0.05).

**TABLE 2** | List of circRNA/miRNA/mRNA targets with a reported role in epilepsy.

| Target       | Gene description               | Role in epilepsy                                                                  | References           |
|--------------|--------------------------------|-----------------------------------------------------------------------------------|----------------------|
| <i>Drd2</i>  | Dopamine receptor D2           | Increased hippocampal death in <i>Drd2</i> <sup>-/-</sup> mice                    | Bozzi et al. (2000)  |
| <i>Tll1</i>  | Tolloid-like 1                 | Increased transcript degradation by NMD upon SE                                   | Mooney et al. (2017) |
| <i>Cd200</i> | Cluster of differentiation 200 | mRNA downregulation in epileptogenic lesions of Focal cortical dysplasia type IIb | Sun et al. (2016)    |

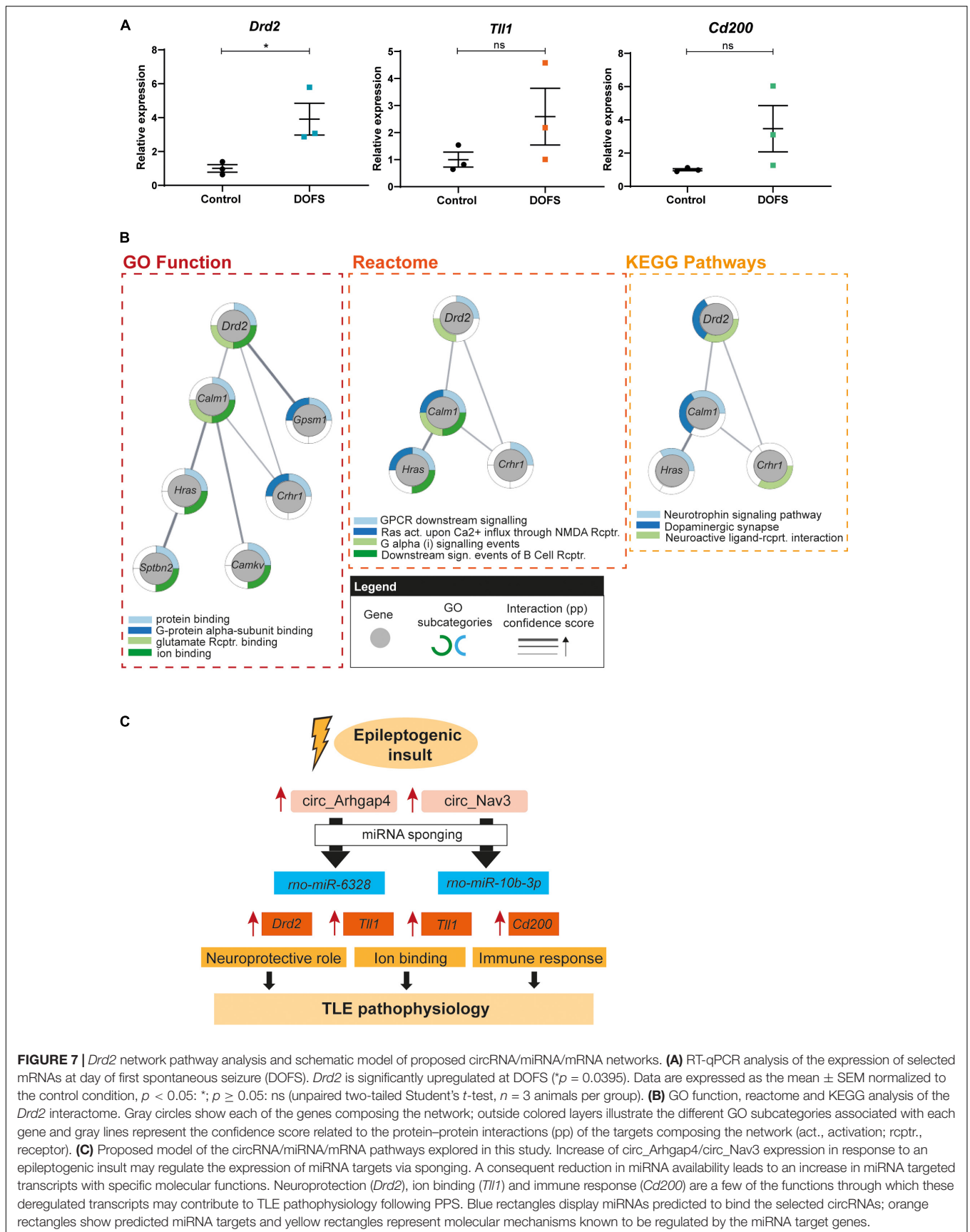
and in a mouse model (Gong et al., 2018; Lee et al., 2018; Li J. et al., 2018). Here, we used RNA-seq to explore circRNA expression at different stages from the initiation of experimental TLE through to the chronic stages, when spontaneous seizures are well established. Interestingly, deregulation of circRNA expression was most prominent at the DOFS, with 218 DE circRNAs. Another recent study using a mouse model of epilepsy detected 48 DE genes at 60 days after pilocarpine-induced SE (chronic epilepsy) (Lee et al., 2018). Although this study used microarray technology to probe circRNA expression, the limited number of differently expressed circRNAs at late (and very early) stages of experimental epilepsy in mouse and rat models may hint at specific regulation of circRNA expression during the transition from epileptogenesis to chronic epilepsy. In our study, the majority of deregulated circRNAs (68%) displayed increased expression. This is consistent with observations from a recent study using a pilocarpine mouse model (60.5% upregulated circRNAs) (Lee et al., 2018). In contrast, in brain tissue from TLE patients, circRNA expression was predominantly downregulated among the DE targets (57.5% downregulated circRNAs) (Li J. et al., 2018). This apparent discrepancy may be explained by the fact that brain material from TLE patients often represents the “end stage” of the disease, which is characterized by massive cell death and other cellular changes that could cause reduced tissue expression of specific circRNAs and which typically occurs after several decades of uncontrolled epilepsy.

Multiple studies have reported circRNA expression regulation independent of that of the corresponding linear transcripts (Jeck et al., 2013; Ashwal-Fluss et al., 2014; Rybak-Wolf et al., 2014; Xu et al., 2018). However, also concomitant changes in the expression of both types of RNA are reported, e.g., during neuronal differentiation (Salzman et al., 2013; Rybak-Wolf et al., 2014). We validated the upregulation of circ\_Arhgap4 and circ\_Nav3 at the DOFS and found similar regulation of their circular and linear host transcripts. This is in contrast with earlier findings, in which no obvious correlation was observed between specific circRNAs and the expression of their parental genes in mTLE (Gray et al., 2020). A positive correlation in the expression of circRNA and mRNA species suggests that the RNA changes are a consequence of transcriptional activation of these genes rather than an alteration of splicing events that lead to circRNA formation (Jeck and Sharpless, 2014). Further, it may indicate a role for these specific circRNAs in regulating host gene expression (Barrett and Salzman, 2016). Since we were able to replicate the predicted RNA-seq changes of circ\_Arhgap4 and circ\_Nav3 by RT-qPCR analysis we decided to focus on these two candidates. Although we focused on rat-specific and rat and human conserved circRNAs, given the fact that those were the most deregulated circular transcripts, circ\_Nav3 isoforms other

than the one studied were detected by RNA-seq and found to be differentially expressed in DOFS samples. These isoforms are conserved in rodents and humans, which highlights the relevance of *Nav3* circular transcripts in epilepsy and could be further explored.

Mossy fiber growth of DG granule cells and reactive astrogliosis are hallmarks of TLE. Aberrant sprouting is characterized by the projection of mossy fibers from the hilus through the granule layer thereby re-innervating other regions of the DG (Proper et al., 2000). This feature can be found in TLE patients but also in rats that are treated with kainic acid or pilocarpine, and in the PPS rat model used in our study (Tauck and Nadlers, 1985; Okazaki et al., 1999; Proper et al., 2000; Norwood et al., 2010). This mossy fiber sprouting enhances the excitatory loop in dentate granule cells facilitating electrical discharges and, eventually, seizure propagation (Okazaki et al., 1999). Additional observations from tissue of epileptic patients and animal models of epilepsy show that glial cells undergo marked morphological and biochemical alterations that are associated with changes in the expression of astrocytic ion channels (Niquet et al., 1994; Beach et al., 1995; Jacobs et al., 1996; Bordey and Sontheimer, 1998). Interestingly, *Arhgap4* encodes for ARHGAP4, a Rho GTPase activating protein (GAP) that inhibits hippocampal axon growth following overexpression (Vogt et al., 2007). NAV3 is expressed in the outer nuclear membrane of neurons and its expression is induced in reactive astrocytes and neurons following brain injury (Coy et al., 2002). It is therefore possible that the observed enhanced expression of *Arhgap4* and *Nav3* transcripts may contribute to the pathogenesis of TLE. While additional experimental work is needed to test this model, we further explored a possible role of enhanced circ\_Arhgap4 and circ\_Nav3 expression using gene expression analysis and bioinformatics approaches.

Several circRNAs have been shown to act as miRNA sponges via MRE sites (Hansen et al., 2013; Memczak et al., 2013; Thomas and Sætrom, 2014). Our analysis showed that circ\_Arhgap4 and circ\_Nav3 are predicted to interact with *miR-6328* and *miR-10b-3p*, respectively, and may therefore indirectly regulate expression of *miR-6328* and *miR-10b-3p* targets. Notably, neither *miR-6328* nor *miR-10b-3p* were found among the DE miRNAs at DOFS (data not shown), suggesting sponging by circ\_Arhgap4 and circ\_Nav3 does not impact miRNA expression in this specific context. *miR-6328* was identified as a rat-specific miRNA derived from intronic regions of chromosome 20 and its functions are unknown (Clokic et al., 2012). On the other hand, the expression of *miR-10b-3p*, conserved across rodents and humans, is increased in rat brains undergoing stress-induced depression or decreased in rats exposed to cold stress and in regions of brain damage following ischemia (Zhen et al., 2017; Duan et al., 2019;



Fang et al., 2020). Even though no link between *miR-10b-3p* and epilepsy has been established so far, the 5p strand of *miR-10b* is linked to epilepsy. *miR-10b-5p* expression is deregulated in several epilepsy animal models and patients (Liu et al., 2010; Hu et al., 2011; Jimenez-Mateos et al., 2012; Kaalund et al., 2014), suggesting a function for the *miR-10* gene family in TLE.

To investigate a potential involvement of circ\_Arhgap4 and circ\_Nav3, and their predicted miRNA targets in TLE, bioinformatics analysis was used to identify potential *miR-6328* and *miR-10b-3p* targets followed by network analysis of the circRNA/miRNA/mRNA axis. The GO terms retrieved by the functional enrichment analysis of *miR-6328/miR-10b-3p* targets included 'signaling,' 'response to stimulus,' and 'regulation of biological processes.' A possible explanation for this finding is that the observed changes reflect a response to circRNA deregulation as a result of altered neuronal activity. This is in line with the observed enhanced expression of circRNAs at the DOFS and with several studies reporting the regulation of circRNA expression in response to neuronal activity and their synaptic enrichment (Rybak-Wolf et al., 2014; You et al., 2015; Xu et al., 2018). Of the predicted miRNA targets, we found significant upregulation of *Drd2* at the DOFS. *Drd2* encodes dopamine receptor D2 (D2R) and its expression is predicted to be controlled by *miR-6328*, a miRNA bound by circ\_Arhgap4 (Bunzow et al., 1988; Dal Toso et al., 1989). GO Function, Reactome and KEGG pathway analyses revealed an association of *Drd2* with glutamate receptor binding, signaling events, dopaminergic synapse and neuroactive ligand-receptor interactions. Regulation of D2R surface expression in the DG has been linked to synaptic plasticity and memory formation in mice, processes known to be deregulated in epilepsy (Reid and Stewart, 1997; Saab et al., 2009). The specific role of D2 receptors in epilepsy has been extensively investigated in both animal and human studies (Starr, 1996). Inhibition of glutamatergic neurotransmission, susceptibility to KA-induced seizures and regulation of excitotoxicity in the brain are some of the mechanisms previously associated with D2R deregulation. Previous reports have shown that the absence of D2R (*Drd2*<sup>-/-</sup> mice) leads to a lower seizure threshold and increased neurotoxicity in response to treatment with both kainic acid and pilocarpine in comparison to wild-type mice (Bozzi et al., 2000; Bozzi and Borrelli, 2002). These data support the idea that D2R may act as a neuroprotective agent by reducing seizure activity and extensive hippocampal neuronal death (Starr, 1996; Bozzi et al., 2000; Bozzi and Borrelli, 2002; Brodie et al., 2016). Increased expression of *Drd2* as reported here may reflect a protective response against PPS-induced neurodegeneration during early epileptogenesis. Overall, our data supports a model in which upregulation of circ\_Arhgap4 may reduce the availability of *miR-6328* leading to an increase of D2R, which may trigger protection against epilepsy-associated changes.

Most circRNAs identified here only contain one or a few predicted miRNA binding sites. With the exception of Cdr1as (which contains over 70 *miR-7* binding sites) only few circRNAs contain multiple binding sites for a particular miRNA (Guo et al., 2014). Currently, it is suggested that the abundance of circRNA and miRNA should be similar in order for the sponging process

to be considered effective (Guria et al., 2020). This mechanism can be achieved either by a high number of binding sites for a specific miRNA or by an increase in the number of circRNA copies (Zheng et al., 2016). Interestingly, subsets of circRNAs can be highly enriched in cellular compartments, such as synapses (Rybak-Wolf et al., 2014; You et al., 2015), thereby creating an increased local concentration. It is also possible that the circ\_Arhgap4/circ\_Nav3 axis exerts an effect on *Drd2* and other targets via different mechanisms than miRNA sponging, such as binding to RBPs or transcriptional regulation (Lasda and Parker, 2014). As analysis of regulatory circRNA/miRNA/mRNA networks relies on bioinformatics and predictions further work is necessary to explore the effects of circ\_Arhgap4 on *miR-6328* expression levels and unravel the biological processes associated with the circ\_Arhgap4/*miR-6328/Drd2* network.

## CONCLUSION

Our study is the first to profile circRNA expression at different stages of experimental epilepsy. We show that circRNA expression is actively regulated during the process of epileptogenesis leading to epilepsy. These observations support a model in which enhanced neuronal activity due to the occurrence of seizures triggers the expression of circRNAs which could ultimately contribute to the pathogenic process of TLE (Figure 7C). The events surrounding the transition of a post-insult but pre-epileptic network to a brain thereafter generating recurrent spontaneous seizures are poorly understood. Our results indicate that circRNA expression is markedly deregulated during this transition. Interestingly, circRNAs and mRNAs but not miRNAs show such enrichment (Venø et al., 2020). If changes in circRNA expression are an essential feature of the transition period it offers the potential to intervene at this stage and prevent progression to epilepsy.

## DATA AVAILABILITY STATEMENT

The datasets generated for this study are deposited in the Gene Expression Omnibus (GEO) under the accession number GSE137473.

## ETHICS STATEMENT

The animal studies were reviewed and approved by Animal Ethics Committee of Philips University Marburg, Germany or by Utrecht University, Netherlands.

## AUTHOR CONTRIBUTIONS

AG-D contributed to the methodology, investigation, formal analysis, visualization, and writing – original draft preparation. SB contributed to the methodology, conceptualization, animal work, investigation, and writing – review and editing. BN

contributed to the methodology, and writing – review and editing. MV contributed to the analysis and visualization. DCH, JK, and FR contributed to the resources and writing – review and editing. VRV contributed to the methodology, investigation, formal analysis, visualization, and writing – review and editing. RJP contributed to the conceptualization, resources, writing – review and editing, supervision, and funding acquisition. All authors contributed to the article and approved the submitted version.

## FUNDING

This work was financially supported by the European Union's "Seventh Framework" Program (FP7) under Grant Agreement 602130 (EpimiRNA), the Epilepsiefonds (WAR18-05), Science Foundation Ireland under Grant Number 16/RC/3948 and co-funded under the European Regional Development Fund and by FutureNeuro industry partners (DCH), and the European Union's Horizon 2020 Research and Innovation Program under the Marie Skłodowska-Curie Grant Agreement No. 721890 (circRTrain ITN).

## ACKNOWLEDGMENTS

We thank Nefeli Kakava and Mienke Lujendijk for providing P1 Long Evans rats. We would like to thank the Pasterkamp group members for the scientific discussions and input throughout the project.

## SUPPLEMENTARY MATERIAL

The Supplementary Material for this article can be found online at: <https://www.frontiersin.org/articles/10.3389/fgene.2021.627907/full#supplementary-material>

**Supplementary Figure 1 |** Sequencing validation of circ\_Arhgap4 and circ\_Nav3 back splice junctions. Custom DNA sequencing following RT-qPCR was used to confirm the sequence identity of the back splice junctions of (A) circ\_Arhgap4 and (B) circ\_Nav3 (BSJ, back splice junction).

**Supplementary Table 1 |** circRNAs found after DESeq2 analysis. All circRNAs detected after RNA-seq and found to be differentially expressed by DESeq2 analysis are listed. circRNAs are sorted based on the adjusted *p*-values at DOFS. *N* = 3 animals were used in each group (MRP2, 1 day after PPS; MRP3, 3 days after PPS; MRP4, 10 days after PPS; MRP6, DOFS; MRP7, 30 days after DOFS; MRP8, control; padj, adjusted *p*-value).

**Supplementary Table 2 |** List of oligonucleotides and corresponding sequences used in this study. Primers used for RT-qPCR were designed using the

## REFERENCES

Andersen, C. L., Jensen, J. L., and Ørntoft, T. F. (2004). Normalization of real-time quantitative reverse transcription-PCR data: a model-based variance estimation approach to identify genes suited for normalization, applied to bladder and colon cancer data sets. *Cancer Res.* 64, 5245–5250. doi: 10.1158/0008-5472.CAN-04-0496

Primer-BLAST online tool (<https://www.ncbi.nlm.nih.gov/tools/primer-blast/>) or were obtained from previous publications (*Spidr*, *Ca200*) (Fonken et al., 2018; Mao et al., 2019). The following criteria were applied during the design: oligonucleotide length 18–24 bp; melting temperature (T<sub>m</sub>) 52–64°C; %G/C content 40–60%; minimum self-complementary regions and generation of an amplicon size < 250 bp. All primers were purchased from IDT-DNA.

**Supplementary Table 3 |** NormFinder analysis to identify normalization genes. NormFinder (\*.xla, MS Excel 2003 v0.953) statistics was used to determine the most stable reference gene combination considering the two experimental groups (control and DOFS). NormFinder analysis focused on the intra- and inter-individual expression variation of the transcripts. The best combination of genes is provided given the calculated stability value: the lower the value, the more stable the combination (*β-actin* and *Gapdh* = 0,188). Raw untransformed cycle threshold (Ct) values were used and group identifiers (group id) given to the different groups (C1–3, control = 0, DOFS1–3, DOFS = 1). A spike in derived from *Caenorhabditis elegans* (c.e.) was used during cDNA synthesis in order to control for possible artifacts.

**Supplementary Table 4 |** MiRDB analysis of predicted miRNA binding sites in the circRNA sequence. MiRDB database was used to perform bioinformatics analysis of circRNA and miRNA targets. Initially, 'miRNA custom prediction tool' was used to predict miRNA binding sites (or MREs) present in the circRNA sequences, back-splice junction included. Only predicted miRDB scores > 60 were considered. Selected *rno-miRNAs* were then individually used in the 'target search tool.' Several miRNA targets were retrieved for each miRNA, with predicted 3'UTR binding sites. Only predicted miRDB scores ≥ 80 were considered.

**Supplementary Table 5 |** g:Profiler analysis of circRNA/miRNA/mRNA targets. g:GOST tool of g:Profiler was used to perform functional profiling of the circRNA/miRNA/mRNA targets retrieved by miRDB (miRDB score ≥ 80). Cytoscape interface (Enrichment map) was used to identify GO categories over-represented among the targets. 'Node table > Enrichment' represents all targets found to be enriched in a certain GO class and correspondent statistics. 'Edge table > gene overlap' contains all genes found to be overlapping targets among the GO categories. Existing GO categories were classified and grouped into five general classes according to their functional profiling ("nervous system development," "development and morphogenesis," "neurogenesis," "synapse regulation," and "signaling, response to stimulus and regulation of biological processes") and graphically visualized in Cytoscape. Enrichment was calculated as  $-\log_{10} \text{fdr\_qvalue}$  and enrichment significance considered for  $\text{fdr\_qvalue} < 0.05$  (Node table: EnrichmentMap GS\_DESCR, gene set description; EnrichmentMap:GS\_Type, enrichment nodes; EnrichmentMap GS size, number of genes found in each gene set/GO category;  $\text{fdr\_qvalue}$ , gene set *q*-value. Edge table: shared name, overlapping gene sets/GO categories; EnrichmentMap:similarity\_coefficient, calculated coefficient of the overlap between the two gene sets/GO categories; EnrichmentMap:Overlap\_size, number of genes associated with the overlap of the GO categories).

**Supplementary Table 6 |** Complete annotations of *Drd2* network analysis (KEGG, reactome, GO function). Cytoscape StringApp was used to perform functional enrichment analysis of *Drd2* and interacting genes. The entry list included all circRNA/miRNA/mRNA targets retrieved by miRDB (miRDB score ≥ 80) but only the networks including *Drd2* were considered. All retrieved categories (reactome, KEGG pathways and GO function) subcategories' description and genes found are listed. Enrichment was calculated as  $\log_{10} \text{FDR}$  and statistical significance considered for  $\text{FDR} < 0.05$  (GO, gene ontology; FDR, false discovery rate).

Ashwal-Fluss, R., Meyer, M., Pamudurti, N. R., Ivanov, A., Bartok, O., Hanan, M., et al. (2014). CircRNA biogenesis competes with Pre-mRNA splicing. *Mol. Cell* 56, 55–66. doi: 10.1016/j.molcel.2014.08.019

Barker-Haliski, M., and Steve White, H. (2015). Glutamatergic mechanisms associated with seizures and epilepsy. *Cold Spring Harb. Perspect. Med.* 5:a022863. doi: 10.1101/cshperspect.a022863

- Barrett, S. P., and Salzman, J. (2016). Circular RNAs: analysis, expression and potential functions. *Development* 143, 1838–1847. doi: 10.1242/dev.128074
- Bartel, D. P. (2009). MicroRNAs: target recognition and regulatory functions. *Cell* 136, 215–233. doi: 10.1016/j.cell.2009.01.002
- Beach, T. G., Woodhurst, W. B., Macdonald, D. B., and Jones, M. W. (1995). Reactive microglia in hippocampal sclerosis associated with human temporal lobe epilepsy. *Neurosci. Lett.* 191, 27–30. doi: 10.1016/0304-3940(94)11548-11541
- Benbadis, S. R., and Semah, F. (1999). Is the underlying cause of epilepsy a major prognostic factor for recurrence? [6] (multiple letters). *Neurology* 53:440. doi: 10.1212/WNL.53.2.437-e
- Bender, R. A., Dubé, C., and Baram, T. Z. (2004). Febrile seizures and mechanisms of epileptogenesis: insights from an animal model. *Adv. Exp. Med. Biol.* 548, 213–225. doi: 10.1007/978-1-4757-6376-8\_15
- Boon, P., Raedt, R., De Herdt, V., Wyckhuys, T., and Vonck, K. (2009). Electrical stimulation for the treatment of epilepsy. *Neurotherapeutics* 6, 218–227. doi: 10.1016/j.nurt.2008.12.003
- Bordey, A., and Sontheimer, H. (1998). Properties of human glial cells associated with epileptic seizure foci. *Epilepsy Res.* 32, 286–303. doi: 10.1016/S0920-1211(98)00059-x
- Bozzi, Y., and Borrelli, E. (2002). Dopamine D2 receptor signaling controls neuronal cell death induced by muscarinic and glutamatergic drugs. *Mol. Cell. Neurosci.* 19, 263–271. doi: 10.1006/mcne.2001.1064
- Bozzi, Y., and Borrelli, E. (2013). The role of dopamine signaling in epileptogenesis. *Front. Cell. Neurosci.* 7:157. doi: 10.3389/fncel.2013.00157
- Bozzi, Y., Vallone, D., and Borrelli, E. (2000). Neuroprotective role of dopamine against hippocampal cell death. *J. Neurosci.* 20, 8643–8649.
- Brodie, M. J., Besag, F., Ettinger, A. B., Mula, M., Gobbi, G., Comai, S., et al. (2016). Epilepsy, antiepileptic drugs, and aggression: an evidence-based review. *Pharmacol. Rev.* 68, 563–602. doi: 10.1124/pr.115.012021
- Bunzow, J. R., Van Tol, H. H., Grandy, D. K., Albert, P., Salon, J., MacDonald, C., et al. (1988). Cloning and expression of a rat D2 dopamine receptor cDNA. *Nature* 336, 783–787. doi: 10.1038/336783a0
- Calebiro, D., Nikolaev, V. O., Persani, L., and Lohse, M. J. (2010). Signaling by internalized G-protein-coupled receptors. *Trends Pharmacol. Sci.* 31, 221–228. doi: 10.1016/j.tips.2010.02.002
- Chen, Y., and Wang, X. (2020). miRDB: an online database for prediction of functional microRNA targets. *Nucleic Acids Res.* 48, D127–D131. doi: 10.1093/nar/gkz757
- Clokic, S. J. H., Lau, P., Kim, H. H., Coon, S. L., and Klein, D. C. (2012). MicroRNAs in the pineal Gland: miR-483 regulates melatonin synthesis by targeting arylalkylamine N-acetyltransferase. *J. Biol. Chem.* 287, 25312–25324. doi: 10.1074/jbc.M112.356733
- Cortés-López, M., and Miura, P. (2016). Emerging functions of circular RNAs. *Yale J. Biol. Med.* 89, 527–537. doi: 10.1186/s12929-019-0523-z
- Costard, L. S., Neubert, V., Venø, M. T., Su, J., Kjems, J., Connolly, N. M. C., et al. (2019). Electrical stimulation of the ventral hippocampal commissure delays experimental epilepsy and is associated with altered microRNA expression. *Brain Stimul.* 12, 1390–1401. doi: 10.1016/j.brs.2019.06.009
- Coy, J. F., Wiemann, S., Bechmann, I., Bächner, D., Nitsch, R., Kretz, O., et al. (2002). Pore membrane and/or filament interacting like protein 1 (POMFIL1) is predominantly expressed in the nervous system and encodes different protein isoforms. *Gene* 290, 73–94. doi: 10.1016/S0378-1119(02)00567-x
- Dal Toso, R., Sommer, B., Ewert, M., Herb, A., Pritchett, D. B., Bach, A., et al. (1989). The dopamine D2 receptor: two molecular forms generated by alternative splicing. *EMBO J.* 8, 4025–4034.
- Dalby, N. O., and Mody, I. (2001). The process of epileptogenesis: a pathophysiological approach. *Curr. Opin. Neurol.* 14, 187–192. doi: 10.1097/00019052-200104000-200104009
- Devinsky, O., Vezzani, A., O'Brien, T. J., Jette, N., Scheffer, I. E., De Curtis, M., et al. (2018). Epilepsy. *Nat. Rev. Dis. Prim.* 4:18024. doi: 10.1038/nrdp.2018.24
- Doncheva, N. T., Morris, J. H., Gorodkin, J., and Jensen, L. J. (2019). Cytoscape stringapp: network analysis and visualization of proteomics data. *J. Proteome Res.* 18, 623–632. doi: 10.1021/acs.jproteome.8b00702
- Duan, X., Gan, J., Peng, D., Bao, Q., Xiao, L., Wei, L., et al. (2019). Identification and functional analysis of microRNAs in rats following focal cerebral ischemia injury. *Mol. Med. Rep.* 49, 4175–4184. doi: 10.3892/mmr.2019.10073
- Duncan, J. S., Sander, J. W., Sisodiya, S. M., and Walker, M. C. (2006). Adult epilepsy. *Lancet* 367, 1087–1100. doi: 10.1016/S0140-6736(06)68477-68478
- Fang, K., Xu, J. X., Chen, X. X., Gao, X. R., Huang, L. L., Du, A. Q., et al. (2020). Differential serum exosome microRNA profile in a stress-induced depression rat model. *J. Affect. Disord.* 274, 144–158. doi: 10.1016/j.jad.2020.05.017
- Fonken, L. K., Frank, M. G., Gaudet, A. D., D'Angelo, H. M., Daut, R. A., Hampson, E. C., et al. (2018). Neuroinflammatory priming to stress is differentially regulated in male and female rats. *Brain. Behav. Immun.* 70, 257–267. doi: 10.1016/j.bbi.2018.03.005
- Frotscher, M., Soriano, E., and Misgeld, U. (1994). Divergence of hippocampal mossy fibers. *SYNAPSE* 16, 148–160. doi: 10.1002/syn.890160208
- Fu, Y., Wu, Z., Guo, Z., Chen, L., Ma, Y., Wang, Z., et al. (2020). Systems-level analysis identifies key regulators driving epileptogenesis in temporal lobe epilepsy. *Genomics* 112, 1768–1780. doi: 10.1016/j.ygeno.2019.09.020
- Glazar, P., Papavasileiou, P., and Rajewsky, N. (2014). CircBase: a database for circular RNAs. *RNA* 20, 1666–1670. doi: 10.1261/rna.043687.113
- Gong, G. H., An, F. M., Wang, Y., Bian, M., Wang, D., and Wei, C. X. (2018). Comprehensive circular RNA profiling reveals the regulatory role of the CircRNA-0067835/miR-155 pathway in temporal lobe epilepsy. *Cell. Physiol. Biochem.* 51, 1399–1409. doi: 10.1159/000495589
- Gray, L. G., Mills, J. D., Curry-Hyde, A., Devore, S., Friedman, D., Thom, M., et al. (2020). Identification of specific circular RNA expression patterns and MicroRNA interaction networks in mesial temporal lobe epilepsy. *Front. Genet.* 11:564301. doi: 10.3389/fgene.2020.564301
- Guelfi, S., Botia, J. A., Thom, M., Ramasamy, A., Perona, M., Stanyer, L., et al. (2019). Transcriptomic and genetic analyses reveal potential causal drivers for intractable partial epilepsy. *Brain* 142, 1616–1630. doi: 10.1093/brain/awz074
- Guo, J. U., Agarwal, V., Guo, H., and Bartel, D. P. (2014). Expanded identification and characterization of mammalian circular RNAs. *Genome Biol.* 15:409. doi: 10.1186/s13059-014-0409-z
- Guria, A., Sharma, P., Natesan, S., and Pandi, G. (2020). Circular RNAs—the road less traveled. *Front. Mol. Biosci.* 6:146. doi: 10.3389/fmolb.2019.00146
- Hanan, M., Soreq, H., and Kadener, S. (2017). CircRNAs in the brain. *RNA Biol.* 14, 1028–1034. doi: 10.1080/15476286.2016.1255398
- Hansen, T. B., Jensen, T. I., Clausen, B. H., Bramsen, J. B., Finsen, B., Damgaard, C. K., et al. (2013). Natural RNA circles function as efficient microRNA sponges. *Nature* 495, 384–388. doi: 10.1038/nature11993
- Hansen, T. B., Wiklund, E. D., Bramsen, J. B., Villadsen, S. B., Statham, A. L., Clark, S. J., et al. (2011). miRNA-dependent gene silencing involving Ago2-mediated cleavage of a circular antisense RNA. *EMBO J.* 30, 4414–4422. doi: 10.1038/emboj.2011.359
- Henshall, D. C., Hamer, H. M., Pasterkamp, R. J., Goldstein, D. B., Kjems, J., Prehn, J. H. M., et al. (2016). MicroRNAs in epilepsy: pathophysiology and clinical utility. *Lancet Neurol.* 15, 1368–1376. doi: 10.1016/S1474-4422(16)30246-30240
- Henshall, D. C., and Kobow, K. (2015). Epigenetics and epilepsy. *Cold Spring Harb. Perspect. Med.* 5:a022731. doi: 10.1101/cshperspect.a022731
- Hinrichs, A. S., Karolchik, D., Baertsch, R., Barber, G. P., Bejerano, G., Clawson, H., et al. (2006). The UCSC genome browser database: update 2006. *Nucleic Acids Res.* 34, D590–D598. doi: 10.1093/nar/gkj144
- Hu, K., Zhang, C., Long, L., Long, X., Feng, L., Li, Y., et al. (2011). Expression profile of microRNAs in rat hippocampus following lithium-pilocarpine-induced status epilepticus. *Neurosci. Lett.* 488, 252–257. doi: 10.1016/j.neulet.2010.11.040
- Jacobs, K. M., Gutnick, M. J., and Prince, D. A. (1996). Hyperexcitability in a model of cortical maldevelopment. *Cereb. Cortex* 6, 514–523. doi: 10.1093/cercor/6.3.514
- Jeck, W. R., and Sharpless, N. E. (2014). Detecting and characterizing circular RNAs. *Nat. Biotechnol.* 32, 453–461. doi: 10.1038/nbt.2890
- Jeck, W. R., Sorrentino, J. A., Wang, K., Slevin, M. K., Burd, C. E., Liu, J., et al. (2013). Circular RNAs are abundant, conserved, and associated with ALU repeats. *RNA* 19, 141–157. doi: 10.1261/rna.035667.112
- Jimenez-Mateos, E. M., Engel, T., Merino-Serrais, P., McKiernan, R. C., Tanaka, K., Mouri, G., et al. (2012). Silencing microRNA-134 produces neuroprotective and prolonged seizure-suppressive effects. *Nat. Med.* 18, 1087–1094. doi: 10.1038/nm.2834

- Kaalund, S. S., Venø, M. T., Bak, M., Møller, R. S., Laursen, H., Madsen, F., et al. (2014). Aberrant expression of miR-218 and miR-204 in human mesial temporal lobe epilepsy and hippocampal sclerosis - Convergence on axonal guidance. *Epilepsia* 55, 2017–2027. doi: 10.1111/epi.12839
- Kan, A. A., Van Erp, S., Derijck, A. A. H. A., De Wit, M., Hessel, E. V. S., O'Duibhir, E., et al. (2012). Genome-wide microRNA profiling of human temporal lobe epilepsy identifies modulators of the immune response. *Cell. Mol. Life Sci.* 69, 3127–3145. doi: 10.1007/s00018-012-0992-997
- Kent, W. J. (2002). BLAT—The BLAST-Like alignment tool. *Genome Res.* 12, 656–664. doi: 10.1101/gr.229202
- Kristensen, L. S., Andersen, M. S., Stagsted, L. V. W., Ebbesen, K. K., Hansen, T. B., and Kjems, J. (2019). The biogenesis, biology and characterization of circular RNAs. *Nat. Rev. Genet.* 20, 675–691. doi: 10.1038/s41576-019-0158-157
- Kurita, T., Sakurai, K., Takeda, Y., Horinouchi, T., and Kusumi, I. (2016). Very long-term outcome of non-surgically treated patients with temporal lobe epilepsy with hippocampal sclerosis: a retrospective study. *PLoS One* 11:e0159464. doi: 10.1371/journal.pone.0159464
- Langmead, B., Trapnell, C., Pop, M., and Salzberg, S. L. (2009). Ultrafast and memory-efficient alignment of short DNA sequences to the human genome. *Genome Biol.* 10:R25. doi: 10.1186/gb-2009-10-3-r25
- Lasda, E., and Parker, R. (2014). Circular RNAs: diversity of form and function. *RNA* 20, 1829–1842. doi: 10.1261/rna.047126.114
- Lee, W.-J., Moon, J., Jeon, D., Kim, T.-J., Yoo, J.-S., Park, D.-K., et al. (2018). Possible epigenetic regulatory effect of dysregulated circular RNAs in epilepsy. *PLoS One* 13:e0209829. doi: 10.1371/journal.pone.0209829
- Li, J., Lin, H., Sun, Z., Kong, G., Yan, X., Wang, Y., et al. (2018). High-Throughput data of circular RNA profiles in human temporal cortex tissue reveals novel insights into temporal lobe epilepsy. *Cell. Physiol. Biochem.* 45, 677–691. doi: 10.1159/000487161
- Li, X., Yang, L., and Chen, L. L. (2018). The biogenesis, Functions, and Challenges of Circular RNAs. *Mol. Cell* 71, 428–442. doi: 10.1016/j.molcel.2018.06.034
- Liu, D. Z., Tian, Y., Ander, B. P., Xu, H., Stamova, B. S., Zhan, X., et al. (2010). Brain and blood microRNA expression profiling of ischemic stroke, intracerebral hemorrhage, and kainate seizures. *J. Cereb. Blood Flow Metab.* 30, 92–101. doi: 10.1038/jcbfm.2009.186
- Liu, W., and Wang, X. (2019). Prediction of functional microRNA targets by integrative modeling of microRNA binding and target expression data. *Genome Biol.* 20:18. doi: 10.1186/s13059-019-1629-z
- Lluís, Q.-M., and Fellous, M. (2001). The human Y chromosome: the biological role of a “functional wasteland.” *J. Biomed. Biotechnol.* 1, 18–24. doi: 10.1155/S1110724301000080
- Love, M. I., Huber, W., and Anders, S. (2014). Moderated estimation of fold change and dispersion for RNA-seq data with DESeq2. *Genome Biol.* 15:550. doi: 10.1186/s13059-014-0550-558
- Mao, S., Huang, T., Chen, Y., Shen, L., Zhou, S., Zhang, S., et al. (2019). Circ-Sp1dr enhances axon regeneration after peripheral nerve injury. *Cell Death Dis.* 10:787. doi: 10.1038/s41419-019-2027-x
- Martin, M. (2011). Cutadapt removes adapter sequences from high-throughput sequencing reads. *EMBnet. J.* 17, 10–12. doi: 10.14806/ej.17.1.200
- Memczak, S., Jens, M., Elefsinioti, A., Torti, F., Krueger, J., Rybak, A., et al. (2013). Circular RNAs are a large class of animal RNAs with regulatory potency. *Nature* 495, 333–338. doi: 10.1038/nature11928
- Mills, J. D., van Vliet, E. A., Chen, B. J., Janitz, M., Anink, J. J., Baayen, J. C., et al. (2020). Coding and non-coding transcriptome of mesial temporal lobe epilepsy: critical role of small non-coding RNAs. *Neurobiol. Dis.* 134:104612. doi: 10.1016/j.nbd.2019.104612
- Mooney, C. M., Jimenez-Mateos, E. M., Engel, T., Mooney, C., Diviney, M., Venø, M. T., et al. (2017). RNA sequencing of synaptic and cytoplasmic Upf1-bound transcripts supports contribution of nonsense-mediated decay to epileptogenesis. *Sci. Rep.* 7:41517. doi: 10.1038/srep41517
- Ngugi, A. K., Bottomley, C., Kleinschmidt, I., Sander, J. W., and Newton, C. R. (2010). Estimation of the burden of active and life-time epilepsy: a meta-analytic approach. *Epilepsia* 51, 883–890. doi: 10.1111/j.1528-1167.2009.02481.x
- Niquet, J., Ben-ari, Y., and Represa, A. (1994). Glial reaction after seizure induced hippocampal lesion: immunohistochemical characterization of proliferating glial cells. *J. Neurocytol.* 23, 641–656. doi: 10.1007/BF01191558
- Norwood, B. A., Bauer, S., Wegner, S., Hamer, H. M., Oertel, W. H., Sloviter, R. S., et al. (2011). Electrical stimulation-induced seizures in rats: a “dose-response” study on resultant neurodegeneration. *Epilepsia* 52, e109–e112. doi: 10.1111/j.1528-1167.2011.03159.x
- Norwood, B. A., Bumanglag, A. V., Osculati, F., Sbarbati, A., Marzola, P., Nicolato, E., et al. (2010). Classic hippocampal sclerosis and hippocampal onset epilepsy produced by a single cryptic episode of focal hippocampal excitation in awake rats. *J. Comp. Neurol.* 518, 3381–3407. doi: 10.1002/cne.22406
- Okazaki, M. M., Molnar, M., and Nadler, J. V. (1999). Recurrent mossy fiber pathway in rat dentate gyrus: synaptic currents evoked in presence and absence of seizure-induced growth. *J. Neurophysiol.* 81, 1645–1660. doi: 10.1152/jn.1999.81.4.1645
- Ovcharenko, I., Loots, G. G., Nobrega, M. A., Hardison, R. C., Miller, W., and Stubbs, L. (2005). Evolution and functional classification of vertebrate gene deserts. *Genome Res.* 15, 137–145. doi: 10.1101/gr.3015505
- Panda, A. C. (2018). “Circular RNAs Act as miRNA sponges,” in *Circular RNAs: Biogenesis and Functions*, ed. J. Xiao (Singapore: Springer Singapore), 67–79. doi: 10.1007/978-981-13-1426-1\_6
- Proper, E. A., Oestreich, A. B., Jansen, G. H., Veelen, C. W. M. V., Van Rijen, P. C., Gispén, W. H., et al. (2000). Immunohistochemical characterization of mossy fibre sprouting in the hippocampus of patients with pharmaco-resistant temporal lobe epilepsy. *Brain* 123, 19–30. doi: 10.1093/brain/123.1.19
- Raudvere, U., Kolberg, L., Kuzmin, I., Arak, T., Adler, P., Peterson, H., et al. (2019). g:Profiler: a web server for functional enrichment analysis and conversions of gene lists (2019 update). *Nucleic Acids Res.* 47, W191–W198. doi: 10.1093/nar/gkz369
- Reichardt, L. F. (2006). Neurotrophin-regulated signalling pathways. *Philos. Trans. R. Soc. B Biol. Sci.* 361, 1545–1564. doi: 10.1098/rstb.2006.1894
- Reid, I. C., and Stewart, C. A. (1997). Seizures, memory and synaptic plasticity. *Seizure* 6, 351–359. doi: 10.1016/s1059-1311(97)80034-80039
- Reimand, J., Isserlin, R., Voisin, V., Kucera, M., Tannus-Lopes, C., Rostamianfar, A., et al. (2019). Pathway enrichment analysis and visualization of omics data using g:profiler, GSEA, cytoscape and enrichmentmap. *Nat. Protoc.* 14, 482–517. doi: 10.1038/s41596-018-0103-109
- Rong, D., Sun, H., Li, Z., Liu, S., Dong, C., Fu, K., et al. (2017). An emerging function of circRNA-miRNAs-mRNA axis in human diseases. *Oncotarget* 8, 73271–73281. doi: 10.18632/oncotarget.19154
- Rybak-Wolf, A., Stottmeister, C., Glazár, P., Jens, M., Pino, N., Hanan, M., et al. (2014). Circular RNAs in the mammalian brain are highly abundant, conserved, and dynamically expressed. *Mol. Cell* 58, 870–885. doi: 10.1016/j.molcel.2015.03.027
- Saab, B. J., Georgiou, J., Nath, A., Lee, F. J. S., Wang, M., Michalon, A., et al. (2009). NCS-1 in the dentate gyrus promotes exploration, synaptic plasticity, and rapid acquisition of spatial memory. *Neuron* 63, 643–656. doi: 10.1016/j.neuron.2009.08.014
- Salzman, J., Chen, R. E., Olsen, M. N., Wang, P. L., and Brown, P. O. (2013). Cell-Type specific features of circular RNA expression. *PLoS Genet.* 9:e1003777. doi: 10.1371/journal.pgen.1003777
- Schneider, C. A., Rasband, W. S., and Elliceiri, K. W. (2012). NIH Image to ImageJ: 25 years of image analysis. *Nat. Methods* 9, 671–675. doi: 10.1038/nmeth.2089
- Scimemi, A., Schorge, S., Kullmann, D. M., and Walker, M. C. (2006). Epileptogenesis is associated with enhanced glutamatergic transmission in the perforant path. *J. Neurophysiol.* 95, 1213–1220. doi: 10.1152/jn.00680.2005
- Shannon, P., Markiel, A., Ozier, O., Baliga, N. S., Wang, J. T., Ramage, D., et al. (2003). Cytoscape: a software environment for integrated models of biomolecular interaction networks. *Genome Res.* 13, 2498–2504. doi: 10.1101/gr.1239303
- Shao, Y., and Chen, Y. (2017). Pathophysiology and clinical utility of non-coding RNAs in epilepsy. *Front. Mol. Neurosci.* 10:249. doi: 10.3389/fnmol.2017.00249
- Starr, M. S. (1996). The role of dopamine in epilepsy. *SYNAPSE* 22, 159–194.
- Sun, F. J., Zhang, C. Q., Chen, X., Wei, Y. J., Li, S., Liu, S. Y., et al. (2016). Downregulation of CD47 and CD200 in patients with focal cortical dysplasia type IIb and tuberous sclerosis complex. *J. Neuroinflammation* 13:85. doi: 10.1186/s12974-016-0546-2
- Tauk, D. L., and Nadlers, J. V. (1985). Evidence of functional mossy fiber sprouting in hippocampal formation of kainic acid-treated rats. *J. Neurosci.* 5, 1016–1022. doi: 10.1523/JNEUROSCI.05-04-01016.1985
- Thomas, L. F., and Sætrom, P. (2014). Circular RNAs are depleted of polymorphisms at microRNA binding sites. *Bioinformatics* 30, 2243–2246. doi: 10.1093/bioinformatics/btu257

- Van Gassen, K. L. I., De Wit, M., Koerkamp, M. J. A. G., Rensen, M. G. A., Van Rijen, P. C., Holstege, F. C. P., et al. (2008). Possible role of the innate immunity in temporal lobe epilepsy. *Epilepsia* 49, 1055–1065. doi: 10.1111/j.1528-1167.2007.01470.x
- Venø, M. T., Reschke, C. R., Morris, G., Connolly, N. M. C., Su, J., Yan, Y., et al. (2020). A systems approach delivers a functional microRNA catalog and expanded targets for seizure suppression in temporal lobe epilepsy. *Proc. Natl. Acad. Sci. U S A.* 117, 15977–15988. doi: 10.1073/pnas.1919313117/-/DCSupplemental
- Villa, C., Lavitrano, M., and Combi, R. (2019). Long non-coding RNAs and related molecular pathways in the pathogenesis of epilepsy. *Int. J. Mol. Sci.* 20:4898. doi: 10.3390/ijms20194898
- Voglis, G., and Tavernarakis, N. (2006). The role of synaptic ion channels in synaptic plasticity. *EMBO Rep.* 7, 1104–1110. doi: 10.1038/sj.embor.7400830
- Vogt, D. L., Gray, C. D., Scott, W. Y. III, Orellana, S. A., and Malouf, A. T. (2007). Arhgap4 is a novel RhoGAP that mediates inhibition of cell motility and axon outgrowth. *Mol. Cell. Neurosci.* 36, 332–342. doi: 10.1016/j.mcn.2007.07.004
- Wieser, H.-G. (2004). Mesial temporal lobe epilepsy with hippocampal sclerosis. *Epilepsia* 45, 695–714. doi: 10.1111/j.0013-9580.2004.09004.x
- Witter, M. P., Naber, P. A., Van Haften, T., Machielsen, W. C. M., Rombouts, S. A. R. B., Barkhof, F., et al. (2000). Cortico-Hippocampal communication by way of parallel parahippocampal-subicular pathways. *Hippocampus* 10, 398–410.
- Xu, K., Chen, D., Wang, Z., Ma, J., Zhou, J., Chen, N., et al. (2018). Annotation and functional clustering of circRNA expression in rhesus macaque brain during aging. *Cell Discov.* 4:48. doi: 10.1038/s41421-018-0050-51
- You, X., Vlatkovic, I., Babic, A., Will, T., Epstein, I., Tushev, G., et al. (2015). Neural circular RNAs are derived from synaptic genes and regulated by development and plasticity. *Nat. Neurosci.* 18, 603–610. doi: 10.1038/nn.3975
- Zhang, X. O., Wang, H., Bin, Zhang, Y., Lu, X., Chen, L. L., et al. (2014). Complementary sequence-mediated exon circularization. *Cell* 159, 134–147. doi: 10.1016/j.cell.2014.09.001
- Zhen, L., Guo, W., Peng, M., Liu, Y., Zang, S., Ji, H., et al. (2017). Identification of cold-responsive miRNAs in rats by deep sequencing. *J. Therm. Biol.* 66, 114–124. doi: 10.1016/j.jtherbio.2017.03.005
- Zheng, Q., Bao, C., Guo, W., Li, S., Chen, J., Chen, B., et al. (2016). Circular RNA profiling reveals an abundant circHIPK3 that regulates cell growth by sponging multiple miRNAs. *Nat. Commun.* 7:11215. doi: 10.1038/ncomms11215

**Conflict of Interest:** MV was employed by the company Omiics ApS. BN was employed by the companies Expesicor Inc. and FYR Diagnostics.

The remaining authors declare that the research was conducted in the absence of any commercial or financial relationships that could be construed as a potential conflict of interest.

Copyright © 2021 Gomes-Duarte, Bauer, Venø, Norwood, Henshall, Kjems, Rosenow, Vangoor and Pasterkamp. This is an open-access article distributed under the terms of the Creative Commons Attribution License (CC BY). The use, distribution or reproduction in other forums is permitted, provided the original author(s) and the copyright owner(s) are credited and that the original publication in this journal is cited, in accordance with accepted academic practice. No use, distribution or reproduction is permitted which does not comply with these terms.